JOC The Journal of Organic Chemistry

Article

pubs.acs.org/joc

^{13}C-Labeled Idohexopyranosyl Rings: Effects of Methyl Glycosidation and C6 Oxidation on Ring Conformational Equilibria

Bidisha Bose-Basu,[†] Wenhui Zhang,[‡] Jamie L. W. Kennedy,[‡] Matthew J. Hadad,[‡] Ian Carmichael,[§] and Anthony S. Serianni*[,‡]

[†]Department of Chemistry and Physics, Fayetteville State University, Fayetteville, North Carolina 28301, United States

[‡]Department of Chemistry and Biochemistry, and [§]Radiation Laboratory, University of Notre Dame, Notre Dame, Indiana 46556-5670, United States

Supporting Information

ABSTRACT: An ensemble of J_{HH}, J_{CH}, and J_{CC} values was measured in aqueous solutions of methyl α- and β-D-idohexopyranosides containing selective ^{13}C-enrichment at various carbons. By comparing these J-couplings to those reported previously in the α- and β-D-idohexopyranoses, methyl glycosidation was found to affect ring conformational equilibria, with the percentages of $^4C_1$ forms based on $^3J_{HH}$ analysis as follows: α-D-idopyranose, ~18%; methyl α-D-idopyranoside, ~42%; methyl β-D-idopyranoside, ~74%; β-D-idopyranose, 82%. J_{CH} and J_{CC} values were analyzed with assistance from theoretical values obtained from density functional theory (DFT) calculations. Linearized plots of the percentages of $^4C_1$ against limiting J_{CH} and J_{CC} values in the chair forms were used to (a) determine the compatibility of the experimental J_{CH} and J_{CC} values with $^4C_1/^1C_4$ ratios determined from J_{HH} analysis and (b) determine the sensitivity of specific J_{CH} and J_{CC} values to ring conformation. Ring conformational equilibria for methyl idohexopyranosides differ significantly from those predicted from recent molecular dynamics (MD) simulations, indicating that equilibria determined by MD for ring configurations with energetically flat pseudorotational itineraries may not be quantitative. J-couplings in methyl α-L-[6-^{13}C]idopyranosiduronic acid and methyl α-D-[6-^{13}C]glucopyranosiduronic acid were measured as a function of solution pH. The ring conformational equilibrium is pH-dependent in the iduronic acid.

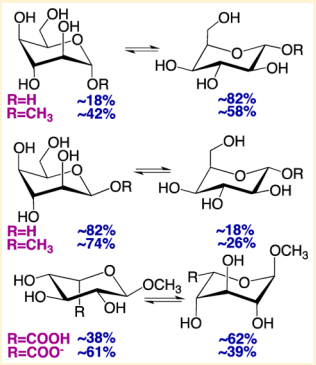

INTRODUCTION

Aldohexopyranosyl rings are important constituents of many biologically important oligo- and polysaccharides.[1,2] These rings contain multiple conformational elements that, like those found in the aldopentofuranosyl rings of DNA and RNA, are interdependent. These elements include exocyclic C−O bond conformation θ (especially important when the C−O bonds are involved in O-glycosidic linkages such as ϕ and ψ),[3] exocyclic hydroxymethyl group (CH_2OH) conformation (rotation about the C5−C6 bond, ω),[4] and pyranosyl ring pseudorotation,[5] characterized by two limiting chair forms denoted $^4C_1$ and $^1C_4$ (Scheme 1). Unlike many biologically important building blocks, aldohexopyranosyl rings are rich in electron lone-pairs (see **2**) that heavily influence their properties. These lone pairs are displayed in specific spatial arrangements determined by their carbon scaffolds. The relative disposition of lone-pair orbitals on these scaffolds not only determines overall molecular dipole moment, which is time-dependent due to C−O bond conformational averaging in solution, but also imparts structural plasticity to the ring caused by 1,2-, 1,3-, and 1,4-lone-pair effects on proximal C−H and C−C bond lengths and other molecular parameters (Scheme 2).[6] The inherent structural, and by inference, chemical and biochemical properties of these rings are strong functions of the relative orientation of their abundant lone-pair orbitals, leading to the expectation that these properties differ for molecules free in solution and in receptor-bound states where these dispositions are rigidified into specific configurations.

Scheme 1. Conformational Elements in Saccharides: Methyl β-D-Galactopyranosyl-(1 →4)-β-D-xylopyranoside (1)

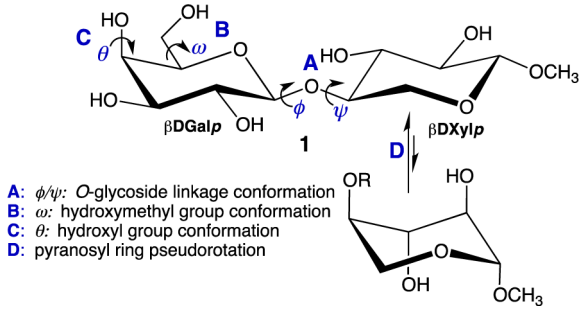

Noncovalent bonding interactions influence the conformational properties of aldohexopyranosyl rings, some intramolecular and others intermolecular, with the latter typically involving solvent water. In the binding site of a receptor, the latter solvent interactions are replaced by new interactions with specific functional groups of the receptor, thus providing a

Received: October 2, 2016
Published: December 22, 2016

DOI: 10.1021/acs.joc.6b02399
J. Org. Chem. 2017, 82, 1356−1370

Scheme 2. Examples of Lone-Pair Effects on C−H Bond Lengths in Saccharides

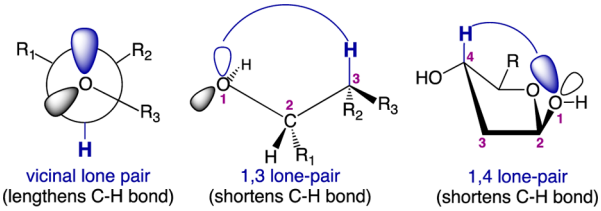

different state of solvation for the ring that in turn affects its structure and reactivity.

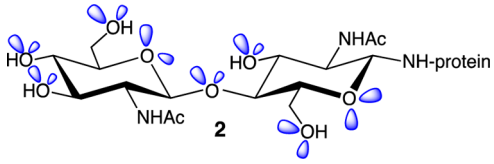

Simple aldohexopyranosyl rings exist in 32 absolute configurations (16 D-series and 16 L-series).[7] Fourteen relative configurations are largely conformationally homogeneous in aqueous solution (i.e., their solutions contain one highly dominant ring conformation or a set of closely related ring conformations). These configurations include *α,β-gluco* **3***α*/*β*, *α,β-manno* **4***α*/*β*, *α,β-galacto* **5***α*/*β*, *α,β-talo* **6***α*/*β*, *α,β-allo* **7***α*/*β*, *β-altro* **8***β*, and *α,β-gulo* **9***α*/*β*. Aldohexopyranosyl rings having the *α-altro* **8***α* and *α,β-ido* **10***α*/*β* configurations are conformationally heterogeneous (*i.e.*, aqueous solutions contain two or more ring conformers that may differ significantly in their overall topologies). Analyses of J_{CC} values,[8−10] J_{CH} values,[11] and $^3J_{HH}$ values[12] support these assignments.

Aldohexopyranosyl ring conformational exchange (pseudorotation) is fast on the NMR time scale at room temperature,[13] and observed NMR parameters such as chemical shifts and *J*-couplings are linearly averaged in accordance with the relative abundances of the contributing conformers in solution. Barriers <8 kcal/mol have been estimated for idohexopyranoside pseudorotation.[14] Idopyranosyl ring pseudorotation thus mimics that of typical aldopentofuranosyl rings.

Studies of conformationally flexible furanosyl and pyranosyl rings and saccharide elements such as exocyclic hydroxymethyl groups and *O*-glycosidic linkages by NMR have benefited from the analysis of NMR spin-coupling (*J*-coupling) ensembles.[3,4] Linear averaging of these parameters simplifies their interpretation when conformational heterogeneity exists, in contrast with the nonlinear averaging of nuclear Overhauser effects (NOEs)[15] and residual dipolar couplings (RDCs)[16,17] that makes them more difficult to use to determine conformer populations in solution. Conventional *J*-coupling analyses focus on homonuclear J_{HH} values, but the latter represent a small percentage of the total *J*-couplings available in saccharides. Simple aldohexopyranosyl rings (e.g., *α,β*-D-glucopyranosyl ring **3**; Scheme 3) contain 50 *J*-couplings (excluding those involving the hydroxyl hydrogens): 7 J_{HH} (14%), 29 J_{CH} (58%), and 14 J_{CC} (28%). Four of the seven J_{HH} values ($^3J_{H1,H2}$, $^3J_{H2,H3}$, $^3J_{H3,H4}$, $^3J_{H4,H5}$) are sensitive to ring conformation, and three ($^3J_{H5,H6R}$, $^3J_{H5,H6S}$, and $^2J_{H6R,H6S}$) are sensitive to exocyclic hydroxymethyl group conformation. Thus, 86% of the available *J*-couplings are routinely unused, in many cases due to a lack of quantitative relationships correlating their magnitudes and signs with saccharide structure.

Scheme 3. Summary of J_{HH}, J_{CH}, and J_{CC} Values in 3*α*/*β*[a]

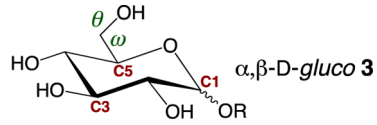

J_{HH}	$^1J_{CH}$	$^2J_{CH}$	$^3J_{CH}$
$^3J_{H1,H2}$	$^1J_{C1,H1}$	$^2J_{C1,H2}$	$^3J_{C1,H3}$
$^3J_{H2,H3}$	$^1J_{C2,H2}$	$^2J_{C2,H1}$	$^3J_{C1,H5}$
$^3J_{H3,H4}$	$^1J_{C3,H3}$	$^2J_{C2,H3}$	$^3J_{C2,H4}$
$^3J_{H4,H5}$	$^1J_{C4,H4}$	$^2J_{C3,H2}$	$^3J_{C3,H1}$
$^3J_{H5,H6R}$	$^1J_{C5,H5}$	$^2J_{C3,H4}$	$^3J_{C3,H5}$
$^3J_{H5,H6S}$	$^1J_{C6,H6R}$	$^2J_{C4,H3}$	$^3J_{C4,H2}$
$^2J_{H6R,H6S}$	$^1J_{C6,H6S}$	$^2J_{C4,H5}$	$^3J_{C4,H6R}$
Total: 7	Total: 7	$^2J_{C5,H4}$	$^3J_{C4,H6S}$
		$^2J_{C5,H6R}$	$^3J_{C5,H1}$
$^1J_{CC}$	$^2J_{CC}$	$^2J_{C5,H6S}$	$^3J_{C5,H3}$
$^1J_{C1,C2}$	$^2J_{C1,C3}$	$^2J_{C6,H5}$	$^3J_{C6,H4}$
$^1J_{C2,C3}$	$^2J_{C1,C5}$	Total: 11	Total: 11
$^1J_{C3,C4}$	$^2J_{C2,C4}$	$^3J_{CC}$	$^{3+3}J_{CC}$
$^1J_{C4,C5}$	$^2J_{C3,C5}$	$^3J_{C1,C6}$	$^{3+3}J_{C1,C4}$
$^1J_{C5,C6}$	$^2J_{C4,C6}$	$^3J_{C3,C6}$	$^{3+3}J_{C2,C5}$
Total: 5	Total: 5	Total: 2	Total: 2

[a]*J*-couplings to hydroxyl hydrogens are not included. Values shown in black relate to pyranosyl ring conformation; values shown in green relate to the conformation about *ω* and/or *θ*.

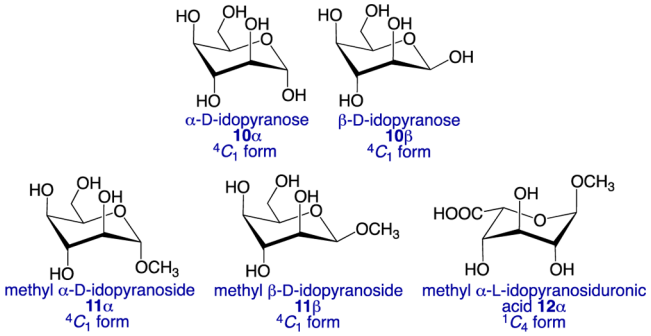

In this report, NMR *J*-couplings (J_{HH}, J_{CH}, and J_{CC}) are used to investigate the conformational properties of D-idopyranoses **10***α* and **10***β* and their methyl glycosides **11***α* and **11***β*, and methyl *α*-L-idopyranosiduronic acid **12***α*, in aqueous solution. The investigation has four aims: (1) to determine the effects of methyl glycosidation and C6 oxidation on idohexopyranosyl ring conformational equilibria; (2) to develop new, and refine prior, general relationships between J_{CH} and J_{CC} values and aldohexopyranosyl ring structure and conformation; (3) to test the accuracy of DFT-calculated NMR *J*-couplings in saccharides; and (4) to validate theoretical predictions of idohexopyranosyl ring conformational equilibria obtained from molecular dynamics (MD) simulations.

RESULTS AND DISCUSSION

A. Defining the Problem. Semiquantitative analyses of intraring $^3J_{HH}$ and $^4J_{HH}$ values and $^3J_{C1,C6}$ values in ^{13}C-labeled D-idopyranoses **10***α* and **10***β* suggest that the preferred ring conformation in aqueous solution depends on anomeric configuration, with **10***α* preferring a $^1C_4$ (or $^1C_4$-like) conformation (~80% $^1C_4$), and **10***β* preferring a $^4C_1$ (or $^4C_1$-like) conformation (~75% $^4C_1$).[18] These data have also suggested that aqueous solutions of **10***α* contain the skew (twist-boat) form $^3S_5$ (equivalent to $^OS_2$) based on a qualitative analysis of $^3J_{H4,H5}$ values (see the related discussion below).[18] Recent DFT calculations[19] on the L-enantiomer of **10***α* have

DOI: 10.1021/acs.joc.6b02399
J. Org. Chem. 2017, 82, 1356−1370

Scheme 4. Preferred Ring Conformers of 10α (L-Isomer) in Solution Predicted from DFT Calculations of Total Energy[19]

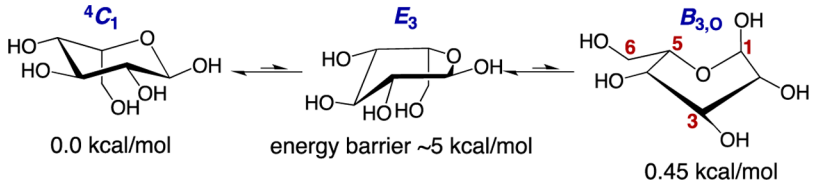

shown that the $^4C_1$ form is most preferred (equivalent to $^1C_4$ in the D-isomer), followed by boat conformer $B_{3,0}$ (equivalent to $^{3,0}B$ in the D-isomer, which is immediately adjacent to $^0S_2$ in the D-aldohexopyranosyl ring pseudorotational itinerary[20]) (Scheme 4). An energy barrier of ~5 kcal/mol was calculated for the interconversion of $^4C_1$ and $B_{3,O}$, with E_3 serving as an intermediate. The H4−C4−C5−H5 torsion angle in $B_{3,O}$ is ~0° compared to ~−60° in $^4C_1$, consistent with the larger than expected $^3J_{H4,H5}$ in **10**α.[18] Thus, NMR[18] and DFT studies[19] draw similar conclusions about the preferred solution conformation of **10**α, and Cremer−Pople parameters calculated by DFT for model structures **11**α_1^{C1}, **11**α_2^{C1}, **11**β_1^{C1}, **11**β_2^{C1}, **11**α_2^{C2}, and **11**β_2^{C2} (see Scheme 5 for definitions and calculations for further discussion of nomenclature) show evidence of skewing toward nonchair forms (Table S1, Supporting Information).

Scheme 5. Model Structures Studied by DFT, Showing Symbolism and Treatment of Exoxyclic Torsion Angles in the Calculations

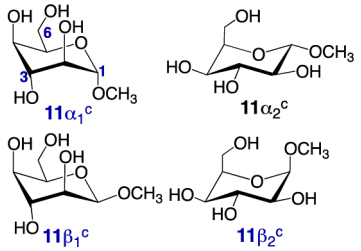

Exocyclic torsions in **11**α_1^{C1}, **11**α_2^{C1}, **11**β_1^{C1} and **11**β_2^{C1} **(Series 1)**
i = initial f = fixed
C2-C1-O1-CH_3 = 180°i
C1-C2-O2-H = 180°f
C2-C3-O3-H = 180°f
C3-C4-O4-H = 180°f
O5-C5-C6-O6 = +60°f (*gt*)
C5-C6-O6-H = 180°f

Exocyclic torsions in **11**α_2^{C2} and **11**β_2^{C2} **(Series 2)**
i = initial f = fixed
C2-C1-O1-CH_3 = 180°i
H2-C2-O2-H = 180°f
H3-C3-O3-H = 180°f
H4-C4-O4-H = 180°f
O5-C5-C6-O6 = +60°f (*gt*)
C5-C6-O6-H = 180°f

Recent 10 μs molecular dynamics (MD) simulations of the L-enantiomers of **11**α and **11**β in explicit water show that the α-pyranoside highly favors $^1C_4$ (~85%) (equivalent to $^4C_1$ of **11**α), while the β-pyranoside almost exclusively prefers $^1C_4$ (99.5%).[14] These MD results are in fair agreement with the above-noted NMR findings for **10**β (75% $^4C_1$ by NMR for **10**β; >99% $^1C_4$ by MD for the β-L-glycoside) but in poor agreement with the NMR findings for **10**α (~80% $^1C_4$ by NMR for **10**α; ~85% $^1C_4$ by MD for the α-L-glycoside). While methyl glycosidation could shift the conformational equilibrium of **10**α, it seems unlikely that this substitution would grossly perturb the equilibrium, despite a presumably stronger *endo*-anomeric effect[21,22] favoring the axial C1−O1 bond in the glycosides.

B. Methyl Glycosidation Affects Idohexopyranosyl Ring Conformational Equilibria: $^3J_{HH}$ Analysis. In light of the ambiguities discussed above, $^3J_{HH}$ values in **10**α, **10**β, **11**α, and **11**β were measured under identical solution conditions (Table 1). Differences between corresponding intraring $^3J_{HH}$ values in the reducing sugar and methyl glycoside of each anomer are small (<|1.8| Hz) but systematic, with all values larger in **10**α than in **11**α and smaller in **10**β than in **11**β (Table 1). Differences in corresponding intraring $^3J_{HH}$ values *between* anomers (excluding $^3J_{H1,H2}$) are larger in the reducing sugars than in the glycosides, implying that glycosidation renders the conformational behaviors of the two anomers more similar.

The above conclusions were tested by quantitative analyses of intraring $^3J_{HH}$, with assistance from DFT-calculated $^3J_{HH}$ values (Table 2). $^3J_{H2,H3}$ and $^3J_{H3,H4}$ differ significantly in the limiting chair conformers as expected. In $^4C_1$, the coupled hydrogens are diequatorial and give *calculated* $^3J_{HH}$ < 2.8 Hz, while in $^1C_4$ they are diaxial and give *calculated* $^3J_{HH}$ > 8.9 Hz. Calculated $^3J_{H2,H3}$ and $^3J_{H3,H4}$ values were averaged in each arrangement (four values in **11**α_1^{C1}/**11**α_2^{C1} and **11**β_1^{C1}/**11**β_2^{C1}; Table 2) to give DFT-calculated limiting $^3J_{HH}^{ee}$ and $^3J_{HH}^{aa}$ values of 2.6 Hz ± 0.5 and 9.2 Hz ± 0.2 Hz, respectively. The larger error in $^3J_{HH}^{ee}$ reflects the wider range of H−C−C−H torsion angles (Table 2) that lie in a steep region of the Karplus curve. *Experimental* $^3J_{H2,H3}$ and $^3J_{H3,H4}$ values in **10**α, **10**β, **11**α and **11**β (Table 1) were then averaged to give 8.0 Hz for **10**α, 3.7 Hz for **10**β, 6.4 Hz for **11**α and 4.3 Hz for **11**β. These averaged experimental values, denoted $^3J_{HH}^{av}$, and the DFT-calculated limiting $^3J_{HH}^{ee}$ and $^3J_{HH}^{aa}$, were used with eq [1] to calculate the fractional populations of $^4C_1$ ($\rho(^4C_1)$) and $^1C_4$ ($\rho(^1C_4)$) forms in aqueous solution.

$$^3J_{HH}^{av} = {}^3J_{HH}^{ee}\,\rho(^4C_1) + {}^3J_{HH}^{aa}\,\rho(^1C_4) \quad (1)$$

This treatment gave the following fractional populations of $^4C_1$ forms: **10**α, ~0.18; **10**β, ~0.82; **11**α, ~0.42; **11**β, ~0.74. These results show that substitution of an OCH_3 group for an OH group at C1 in idohexopyranosyl rings shifts the $^4C_1/^1C_4$ conformational equilibrium significantly, especially for the α-anomer. The $^4C_1$ population increases ~2-fold in the α-anomer, and the $^1C_4$ population increases ~1.4-fold in the β-anomer. These changes are presumably caused by a stronger *endo*-anomeric effect[21,22] in the glycosides relative to the reducing sugars (*i.e.*, methyl glycosidation increases the stability of the chair conformer containing an axial C1−O1 bond). This behavior mimics that of aldopentofuranosyl rings in which methyl glycosidation favors nonplanar conformers bearing axial C1−O1 bonds, at least in some ring configurations.[23] The intrinsic conformational flexibility of idohexopyranosyl rings implies relatively flat energy surfaces along their pseudorotational itineraries that predispose them to conformational shifts

DOI: 10.1021/acs.joc.6b02399
J. Org. Chem. 2017, 82, 1356−1370

Table 1. Experimental J_{HH} Values[a] in 10α, 10β,[b] 11α, and 11β

	compound				Δ values			
J_{HH} (Hz)	**10α**	**11α**	**10β**	**11β**	**10α-11α**	**10β-11β**	**10α-10β**	**11α-11β**
$^3J_{H1,H2}$	6.0	4.3	1.6	1.7	1.7	−0.1		
$^3J_{H2,H3}$	8.1	6.7	3.8	4.1	1.4	−0.3	4.3	2.6
$^3J_{H3,H4}$	7.9	6.1	3.7	4.6	1.8	−0.9	4.2	1.5
$^4J_{H2,H4}$	0	0.3	1.2	0.8	−0.3	0.4	−1.2	−0.5
$^3J_{H4,H5}$	5.0	3.6	1.8	2.5	1.4	−0.7	3.2	1.1
$^3J_{H5,H6}$[c]	8.8	8.6	7.5	8.0	0.2	−0.5	1.3	0.6
$^3J_{H5,H6'}$[c]	3.9	3.8	4.4	4.2	0.1	0.2	−0.5	−0.4
$^2J_{H6,H6'}$[c]	−12.4	−12.2	−11.8	−11.8	−0.2	0	−0.6	−0.4

[a] ±0.2 Hz in ^2H_2O at 25 °C. [b] Values for **10α** and **10β** were taken from ref 18. [c] Stereochemical assignments of the diastereotopic H6*R*/H6*S* hydrogens were not made; H6′ refers to the more shielded hydroxymethyl hydrogen.

Table 2. DFT-Calculated J_{HH}, J_{CH}, and J_{CC} Values in $11\alpha_1^{C1}$, $11\alpha_2^{C1}$, $11\alpha_2^{C2}$, $11\beta_1^{C1}$, $11\beta_2^{C1}$, and $11\beta_2^{C2}$

	model structure					
J-coupling	$11\alpha_1^{C1}$	$11\alpha_2^{C1}$	$11\alpha_2^{C2}$	$11\beta_1^{C1}$	$11\beta_2^{C1}$	$11\beta_2^{C2}$
$^3J_{H1,H2}$	0.8 (−83)[a]	7.8 (−173)	7.6 (−173)	2.1 (54)	4.9 (−51)	4.6 (−51)
$^3J_{H2,H3}$	1.9 (82)	9.0 (175)	9.3 (174)	3.0 (75)	9.4 (180)	9.1 (176)
$^3J_{H3,H4}$	2.8 (−77)	9.4 (−176)	10.1 (−176)	2.6 (−76)	9.2 (−177)	10.3 (179)
$^3J_{H4,H5}$	1.5 (−56)	7.1 (49)	7.2 (50)	1.9 (−50)	7.6 (46)	7.6 (47)
$^1J_{C1,H1}$	172.1	163.5	160.3	161.3	172.9	174.3
$^2J_{C1,H2}$	−1.2	−6.1	−6.4	−0.2	−0.2	0.2
$^2J_{C2,H1}$	−2.1	0.5	1.5	6.9	−1.0	−0.8
$^2J_{C3,H4}$	−4.1	−4.4	−4.0	−3.9	−4.4	−3.8
$^2J_{C6,H5}$	−5.5	−4.9	−5.2	−5.6	−5.1	−5.4
$^3J_{C1,H3}$	4.0 (−159)	1.4 (−67)	1.2 (−69)	5.5 (−168)	1.3 (−64)	1.1 (−66)
$^3J_{C1,H5}$	2.1 (−53)	8.3 (−176)	8.8 (−175)	2.6 (−55)	8.6 (−169)	8.9 (−167)
$^3J_{C2,H4}$	3.5 (164)	1.4 (64)	1.3 (64)	3.7 (164)	1.9 (62)	2.0 (61)
$^3J_{C3,H5}$	1.2 (61)	7.2 (167)	7.4 (167)	0.7 (67)	6.6 (164)	6.6 (164)
$^3J_{C6,H4}$	1.4 (64)	5.5 (169)	5.6 (167)	1.0 (70)	5.6 (165)	5.6 (165)
$^1J_{C5,C6}$	48.5	43.2	42.9	48.0	43.5	43.4
$^2J_{C1,C3}$	−1.5	4.0	6.3	−0.3	−0.7	0.4
$^2J_{C1,C5}$	−2.0	−1.0	−0.9	−0.5	−2.6	−2.6
$^2J_{C2,C4}$	−1.2	+1.9	+3.5	−1.4	+2.6	+4.5
$^3J_{C1,C6}$	2.8 (−170)	1.6 (69)	1.8 (69)	3.4 (−172)	0.2 (76)	0.2 (78)
$^{3+3}J_{C2,C5}$	3.6	−0.1	−0.4	1.1	0.9	0.2
$^3J_{C3,C6}$	2.6 (−179)	1.0 (−73)	0.9 (−74)	2.5 (−174)	0.5 (−77)	0.5 (−77)

[a] In Hz; values in parentheses are torsion angles subtended by the coupled nuclei, in degrees, for the vicinal (three-bond) couplings.

in response to changes in ring substitution. These rings can be regarded as "knife-edge" systems that are delicately balanced energetically and are sensitive to internal, and presumably external, molecular perturbations. Aldohexopyranosyl rings having other relative configurations (e.g., **3**α/β, **4**α/β, **5**α/β) resist these perturbations.

C. Validation of the Effect of Methyl Glycosidation on Idohexopyranosyl Ring Conformational Equilibria: J_{CH} and J_{CC} Analysis. J_{CH} and J_{CC} values in **10**α, **10**β, **11**α, and **11**β (Tables 3 and 4) were examined for their consistency with chair equilibria determined from the $^3J_{HH}$ analysis described in section B. Limiting experimental J_{CH} and J_{CC} values in the $^4C_1$ and $^1C_4$ forms of idohexopyranosyl rings were obtained, when available, from conformationally rigid aldopyranosyl rings containing coupling pathways that mimic those found in idohexopyranosyl rings. Limiting calculated J_{CH} and J_{CC} were obtained from DFT calculations (Table 2). These limiting values and the experimental J_{CH} and J_{CC} values in **10**α, **10**β, **11**α, and **11**β were plotted against the percentages of $^4C_1$ forms in solution determined from the $^3J_{HH}$ analysis. The degree of linearity of the resulting plots was used to test and/or validate the $^4C_1/^1C_4$ equilibria determined from the $^3J_{HH}$ analysis.

C.1. $^{13}C-^1H$ Spin-Couplings. Methyl α-D-mannopyranoside **13** and methyl α-D-arabinopyranoside **14** contain C1−C2 fragments that mimic those found in the $^4C_1$ and $^1C_4$ forms, respectively, of **11**α (Scheme 6). Methyl β-D-mannopyranoside **15** and methyl β-D-arabinopyranoside **16** contain C1−C2 fragments resembling those in the $^4C_1$ and $^1C_4$ forms, respectively, of **11**β (Scheme 6). Since glycosides **13**−**16** highly favor the ring conformations shown in Scheme 6, they provide limiting experimental $^1J_{C1,H1}$ values in the two chair forms of D-idohexopyranosyl rings.[11] Throughout the following discussion, limiting *experimental J*-couplings are shown in plots (Figures 1−5) with green symbols, limiting *calculated J*-couplings with red symbols, and *experimental J*-couplings (*i.e.*, those measured in **10**α/β and **11**α/β) with black symbols. For each color, filled symbols correspond to α-anomers and open symbols to β-anomers.

DOI: 10.1021/acs.joc.6b02399
J. Org. Chem. 2017, 82, 1356−1370

Table 3. Experimental J_{CH} Values[a] in 11α and 11β

	compd	
J-coupling	**11α**	**11β**
$^{1}J_{C1,H1}$	166.5 (165.2)[c]	162.9 (162.8)
$^{2}J_{C1,H2}$	−3.4 (±4.7)	0
$^{3}J_{C1,H3}$	2.7	4.5
$^{3}J_{C1,H5}$	4.0	3.4
$^{3}J_{C1,OCH_3}$	4.5	4.6
$^{1}J_{C2,H2}$	146.4	147.7
$^{2}J_{C2,H1}$	+1.7 (0)	+4.6 (±6.1)
$^{2}J_{C2,H3}$	−4.3	−4.1
$^{3}J_{C2,H4}$	1.2	3.8
$^{1}J_{C3,H3}$	146.8	149.9
$^{2}J_{C3,H2}$	−4.4	−4.7
$^{2}J_{C3,H4}$	−5.4	−4.3
$^{3}J_{C3,H1}$	1.5	0.9
$^{3}J_{C3,H5}$	2.4	1.8
$^{1}J_{C6,H6}$	145.3	146.1
$^{1}J_{C6,H6'}$[b]	142.0	142.0
$^{2}J_{C6,H5}$	−5.1	−4.9
$^{3}J_{C6,H4}$	2.2	1.7

[a]In Hz ± 0.2 Hz; $^{2}H_2O$ solvent at ∼25 °C. [b]H6′ is defined as the more shielded hydroxymethyl hydrogen. [c]Values in parentheses are *J*-couplings observed in the respective reducing sugars, **10**α and **10**β (data taken from ref 18).

Table 4. Experimental J_{CC} Values[a] 11α and 11β

	compd	
J-coupling	**11α**	**11β**
$^{1}J_{C1,C2}$	47.4 (46.2)[b]	45.0 (43.8)
$^{2}J_{C1,OCH_3}$	−2.1	−2.0
$^{2}J_{C1,C3}$	1.5 (±2.5)	∼0 (0)
$^{2}J_{C1,C5}$	1.6 (1.1)	1.0 (0)
$^{3}J_{C1,C6}$	2.4 (1.8)	2.8 (3.1)
$^{3+3}J_{C1,C4}$	br[c] (0)	1.1 (0)
$^{1}J_{C2,C3}$	39.7	nd[d]
$^{2}J_{C2,C4}$	1.1	br
$^{3}J_{C2,OCH_3}$	3.3	3.1
$^{3+3}J_{C2,C5}$	2.2	br
$^{1}J_{C3,C4}$	40.3	40.0
$^{2}J_{C3,C5}$	0	∼0
$^{3}J_{C3,C6}$	1.7 (1.2)	1.9 (2.1)
$^{1}J_{C6,C5}$	43.3 (42.0)	43.7 (44.3)
$^{2}J_{C6,C4}$	∼0 (∼0.7)	∼0

[a]In Hz ± 0.2 Hz; $^{2}H_2O$ solvent at ∼25 °C. [b]Values in parentheses are *J*-couplings observed in the respective reducing sugars, **10**α and **10**β (data taken from ref 18). [c]br, broadened signal, J < 0.6 Hz. [d]nd, not determined.

Good linearity is observed between the experimental $^{1}J_{C1,H1}$ values in **11**α and **11**β (Table 3) and the experimental limiting $^{1}J_{C1,H1}$ values shown in Scheme 6 (Figure 1A). Data for **10**α/β are not shown because $^{1}J_{C1,H1}$ is affected by glycosidation. In this case, limiting *calculated* $^{1}J_{C1,H1}$ values (Table 2) were not included in the plot since they cannot be calculated quantitatively without sampling all hydroxyl conformations in the vicinity of the C−H bond.[4]

Scheme 6. Experimental $^{1}J_{CH}$ Values in 13−16

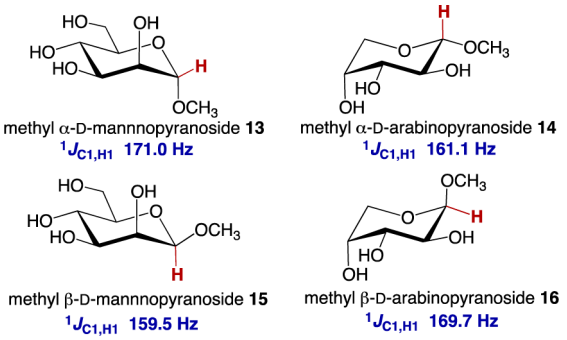

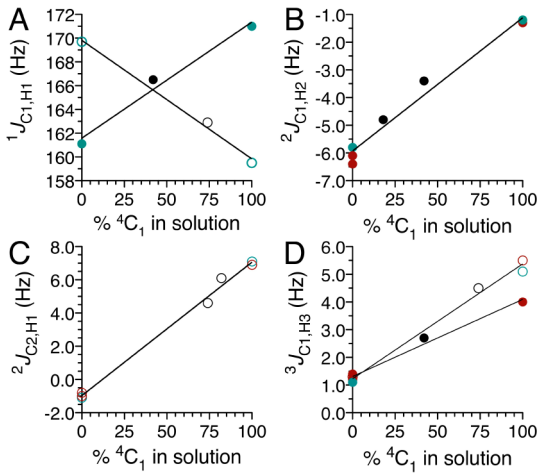

Figure 1. (A) $^{1}J_{C1,H1}$ as a function of % $^{4}C_1$ form in solutions of **11**α and **11**β. (B) $^{2}J_{C1,H2}$ as a function of % $^{4}C_1$ form in solutions of **10**α and **11**α. (C) $^{2}J_{C2,H1}$ as a function of % $^{4}C_1$ form in solutions of **10**β and **11**β. (D) $^{3}J_{C1,H3}$ as a function of % $^{4}C_1$ form in solutions of **11**α and **11**β. In A−D, black symbols, **10**α and **11**α (filled), **10**β and **11**β (open). Green symbols = limiting experimental *J*-couplings; red symbols = limiting calculated *J*-couplings; in both cases, filled = α anomers and open = β-anomers. Linear fits of the data are shown.

$^{2}J_{C1,H2}$ values differ significantly in **10**α and **11**α (Table 3), and limiting experimental values are available in the literature[11] for methyl α-D-mannopyranoside **13** and methyl α-D-arabinopyranoside **14** (Scheme 6).[11] Limiting experimental and calculated $^{2}J_{C1,H2}$ values are in excellent agreement, yielding a dynamic range of ∼5 Hz (Figure 1B). Good linearity is observed between the experimental $^{2}J_{C1,H2}$ values in **10**α and **11**α and the limiting *J*-couplings, with the more negative $^{2}J_{C1,H2}$ in **10**α consistent with a smaller percentage of $^{4}C_1$ form in solution. These results confirm the negative sign of $^{2}J_{C1,H2}$ in methyl α-D-mannopyranoside **13** determined previously.[11] A similar analysis for the β-anomers was not conducted since $^{2}J_{C1,H2}$ in these structures is very small or zero in both chair conformers (Tables 2 and 3).

Limiting experimental $^{2}J_{C2,H1}$ values for **10**β and **11**β obtained from methyl β-D-mannopyranoside **15**[11] and methyl β-D-arabinopyranoside **16**[11] indicate a larger dynamic range (∼7 Hz; Figure 1C) than found for $^{2}J_{C1,H2}$ in **10**α and **11**α (Figure 1B). The agreement between the limiting experimental and calculated $^{2}J_{C2,H1}$ values is excellent, and good linearity is observed when the experimental $^{2}J_{C2,H1}$ values in **10**β and **11**β are included in the plot. These results also provide evidence that the sign of $^{2}J_{C2,H1}$ in methyl β-D-arabinopyranoside **16** is negative.[11] A similar analysis for the α-anomers was not

DOI: 10.1021/acs.joc.6b02399
J. Org. Chem. 2017, 82, 1356−1370

conducted since $^{2}J_{C1,H2}$ in these structures is small in both chair conformers (Tables 2 and 3).

The C1−C2−C3−H3 coupling pathways in methyl β-D-glucopyranoside **17** and methyl β-D-altropyranoside **18** mimic those found in the $^{1}C_4$ and $^{4}C_1$ forms of **11**α and **11**β, respectively. Limiting experimental $^{3}J_{C1,H3}$ values in **17** and **18**[11] were plotted with the limiting calculated $^{3}J_{C1,H3}$ values (Table 2) and the experimental $^{3}J_{C1,H3}$ (Table 3) in **11**α and **11**β (Figure 1D). Good linearity is observed in both data sets, with both lines converging to give a common value of ∼1.2 Hz in the $^{1}C_4$ forms (0% $^{4}C_1$), corresponding to calculated C1−C2−C3−H3 torsion angles of 64−68° (Table 2). However, both lines diverge at 100% $^{4}C_1$, with larger values found in **11**β than in **11**α. The latter difference is attributed to the larger C1−C2−C3−H3 torsion angle in **11**β relative to **11**α (Table 2) and to the effect of the in-plane electronegative substituent at C1 in the β-anomer.[11]

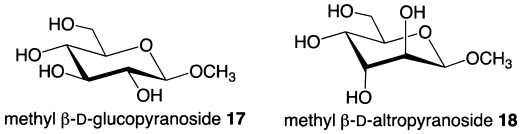

methyl β-D-glucopyranoside **17** methyl β-D-altropyranoside **18**

C.2. $^{13}C-^{13}C$ Spin-Couplings. Experimental $^{1}J_{C5,C6}$ values in the α- and β-D-talopyranoses **19**α/β (45.0 Hz)[24] were used as the limiting experimental values in the $^{4}C_1$ forms of **10**α, **10**β, **11**α, and **11**β. A plot of these limiting values with the experimental $^{1}J_{C5,C6}$ values in **10**α, **10**β, **11**α, and **11**β (Table 4) was approximately linear (Figure 2A). The *y*-intercept of 41.6

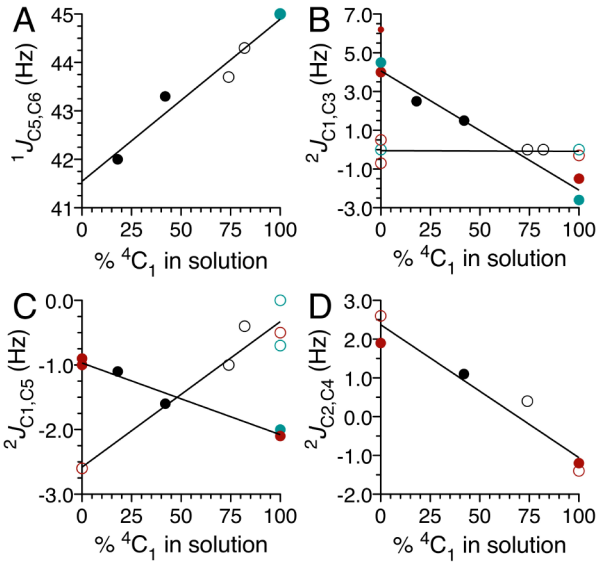

Figure 2. $^{1}J_{C5,C6}$ (A), $^{2}J_{C1,C3}$ (B), and $^{2}J_{C1,C5}$ (C) as a function of % $^{4}C_1$ form in solutions of **10**α, **10**β, **11**α, and **11**β. (D) $^{2}J_{C2,C4}$ as a function of % $^{4}C_1$ form in solutions of **11**α and **11**β. In A, C, and D, the lines represent linear fits of the data. In B, lines represent linear fits of the data except for **11**α_2^{C2} (see text). See Figure 1 for definitions of symbols.

Hz provides an estimate of $^{1}J_{C5,C6}$ in $^{1}C_4$ ring conformers for which an experimental value is currently unavailable. This value (axial C5−C6 bond) is ∼3.5 Hz smaller than that in $^{4}C_1$ forms (equatorial C5−C6 bond) (Figure 2A). DFT-calculated C5−C6 bond lengths in model structures (**11**α_1^{C1}, 1.521 Å; **11**α_2^{C1}, 1.532 Å; **11**β_1^{C1}, 1.521 Å; **11**β_2^{C1}, 1.532 Å; **11**α_2^{C2}, 1.532 Å; **11**β_2^{C2}, 1.532 Å) are ∼0.01 Å shorter for equatorial C5−C6 bonds than for axial C5−C6 bonds. A shorter bond, which implies greater s-character, is associated with a larger $^{1}J_{C5,C6}$. These findings are consistent with the behavior of methyl 2-deoxy-β-D-*erythro*-pentofuranose **20**[25] where ring pseudorotation allows continuous transitions between quasi-axial and quasi-equatorial orientations of the C4−C5 bond. DFT-calculated $^{1}J_{C4,C5}$ values in **20** vary inversely with $r_{C4,C5}$, giving a dynamic range of ∼3.5 Hz associated with a ∼0.013 Å change in bond length (Figure S1; see the Supporting Information). As for $^{1}J_{C1,H1}$ (Figure 1A), limiting *calculated* $^{1}J_{C5,H6}$ values (Table 2) were not included in the plot since they cannot be calculated quantitatively without sampling all hydroxyl conformations in the vicinity of the C−C bond.[10]

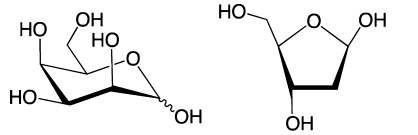

methyl α,β-D-talopyranoses **19**α/β methyl 2-deoxy-β-D-*erythro*-pentofuranose **20**

$^{2}J_{C1,C3}$ values in simple aldopyranosyl rings depend on four structural factors (Scheme S1; see the Supporting Information): (1) the relative orientations of the (terminal) oxygen atoms appended to C1 and C3;[26] (2) C2−O2 bond conformation (θ_2);[27] (3) C1−O1 and C3−O3 bond conformations (θ_1, θ_3);[27] and (4) C2 configuration.[27] Factors 1 and 2 are the strongest and factor 3 the weakest. $^{2}J_{C1,C3}$ values can have positive or negative signs depending on the relative orientation of the terminal C−O bonds; $^{2}J_{C1,C3}$ is most positive (∼+4.5 Hz) when both terminal C−O bonds are equatorial and most negative (∼−2.5 Hz) when both are axial.[26,28,29] The resulting dynamic range (∼7 Hz) renders $^{2}J_{C1,C3}$ one of the most sensitive *J*-couplings to investigate pyranosyl ring conformation, provided that sign information is available.[28,29]

Methyl α-D-allopyranoside **21** and methyl β-D-glucopyranoside **17** provided limiting experimental $^{2}J_{C1,C3}$ values in the $^{4}C_1$ and $^{1}C_4$ forms, respectively, of **10**α and **11**α, and methyl β-D-allopyranoside **22** and methyl α-D-glucopyranoside **23** served the same purpose for **10**β and **11**β. Linear plots of the limiting experimental[10] and calculated $^{2}J_{C1,C3}$ (Table 2) values with the experimental $^{2}J_{C1,C3}$ values (Table 4; Figure 2B) were obtained. $^{2}J_{C1,C3}$ is similar (∼0 Hz) in both chair forms of **10**β and **11**β. However, $^{2}J_{C1,C3}$ is very sensitive to the ring conformation in **10**α and **11**α (dynamic range of ∼6 Hz). The limiting calculated $^{2}J_{C1,C3}$ value in **11**α_2^{C2} was excluded in this plot; this value is associated with a C2−O2 bond conformation (O2*H* *anti* to H2; Scheme 5) in which the lone-pair orbitals on O2 are antiperiplanar to both C−C bonds in the C1−C2−C3 coupling pathway. This arrangement shifts $^{2}J_{C1,C3}$ to a more positive value.[27] Disparities observed between the limiting experimental and calculated $^{2}J_{C1,C3}$ values in the $^{4}C_1$ form of the α-anomer are probably caused by the effects of an axial O2 on $^{2}J_{C1,C3}$ that are not captured by the methyl α-D-allopyranoside mimic.

$^{2}J_{C1,C5}$ values in $^{4}C_1$ forms of D-aldohexopyranosyl rings depend on anomeric configuration, with values of ∼−2 Hz observed in α-anomers (axial C1−O1) and ∼0 Hz in β-anomers (equatorial C1−O1).[26,28,29] This work extends these prior observations to aldohexopyranosyl rings bearing axial C5−C6 bonds. Limiting experimental $^{2}J_{C1,C5}$ values were provided by α-D-mannopyranose **4**α for the $^{4}C_1$ forms of **10**α and **11**α and β-D-mannopyranose **4**β and methyl β-D-

DOI: 10.1021/acs.joc.6b02399
J. Org. Chem. 2017, 82, 1356−1370

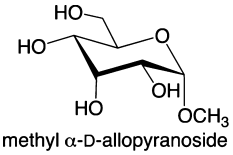

methyl α-D-allopyranoside **21**

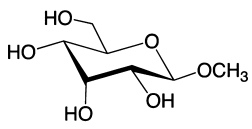

methyl β-D-allopyranoside **22**

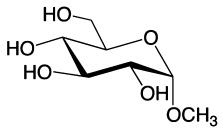

methyl α-D-glucopyranoside **23**

allopyranoside **22** for the $^4C_1$ forms of **10**β and **11**β. Limiting experimental $^2J_{C1,C5}$ values in the $^1C_4$ forms of **10**α/β and **11**α/β are currently unavailable. The limiting experimental and calculated $^2J_{C1,C5}$ values in the $^4C_1$ forms are in reasonable agreement (Figure 2C), considering that the experimental measurements are prone to error because of their small magnitudes. The limiting calculated $^2J_{C1,C5}$ values are ~−1 Hz for $^1C_4$ forms of α-D-idohexopyranosyl rings and ~−2.6 Hz for $^1C_4$ forms of β-D-idohexopyranosyl rings. Limiting calculated $^2J_{C1,C5}$ in $^4C_1$ forms of α-D-idopyranosyl rings differ from limiting $^2J_{C1,C5}$ in $^1C_4$ forms of β-D-idopyranosyl rings despite the presence of axial C1−O1 bonds in both cases. The axial C5−C6 bond in the β-anomers shifts $^2J_{C1,C5}$ to a more negative value by ~0.6 Hz (~−2 Hz to ~−2.6 Hz). A similar shift is observed between β-D-idohexopyranosyl rings ($^4C_1$) and β-D-idohexopyranosyl rings ($^1C_4$) (~−0.5 Hz to ~−1.1 Hz). While the dynamic range for $^2J_{C1,C5}$ is small (<2.5 Hz), plots of the experimental $^2J_{C1,C5}$ values in **10**α and **11**α and in **10**β and **11**β (Table 4) and the corresponding limiting couplings against % $^4C_1$ form in solution are approximately linear (Figure 2C). The plot for the β-anomers indicates that $^2J_{C1,C5}$ in methyl β-D-allopyranoside **22** is probably negative.[10]

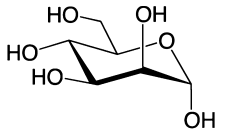

α-D-mannopyranose **4**α

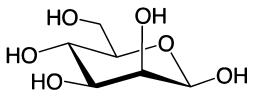

β-D-mannopyranose **4**β

$^2J_{C2,C4}$ values in aldopyranosyl rings exhibit configurational dependencies similar to $^2J_{C1,C3}$, with equatorial C2−O2 and C4−O4 bonds associated with moderately large positive couplings and axial C2−O2 and C4−O4 bonds associated with moderately large negative values.[10] The plot of limiting calculated $^2J_{C2,C4}$ values in **11**α_1^{C1}, **11**α_2^{C1}, **11**β_1^{C1}, and **11**β_2^{C1} and experimental $^2J_{C2,C4}$ values in **11**α and **11**β against % $^4C_1$ form in solution is linear (Figure 2D).

$^3J_{C1,C6}$ values in aldohexopyranosyl rings depend on at least three factors (Scheme 7):[8,9] (a) the C1−O5−C5−C6 torsion angle θ_1; (b) the O1−C1−O5−C5 torsion angle θ_2; and (3) the O5−C5−C6−O6 torsion angle ω. Factor 1 is the Karplus dependency of vicinal $^3J_{COCC}$ values that has been quantified for *O*-glycosidic linkages in oligosaccharides.[3] Factors 2 and 3 describe contributions of in-plane terminal electronegative substituents to $^3J_{COCC}$, with each in-plane substituent contributing ~+0.7 Hz to the observed coupling.[3] An axial O3 also influences $^3J_{C1,C6}$ values for reasons not yet understood.[10] $^3J_{C1,C6}$ is maximal when θ_1, θ_2, and ω are 180° and O3 is equatorial; in cases where θ_1 and θ_2 are fixed and known, $^3J_{C1,C6}$ can serve as an indirect probe of ω. In *ido* rings where $^4C_1$−$^1C_4$ equilibria are of interest, $^3J_{C1,C6}$ serves as a probe of θ_1, which is ~180° and ~+60° in $^4C_1$ and $^1C_4$ forms, respectively, in the D-isomers.

α- (**24**) and β-D-allopyranoses (**25**) provide limiting experimental $^3J_{C1,C6}$ in the $^4C_1$ forms of **10**α/**11**α and **10**β/**11**β, respectively.[8−10] Since limiting experimental $^3J_{C1,C6}$ values are currently unavailable for $^1C_4$ forms, only DFT-calculated limiting values (Table 2) were used in the analysis. Plots of the limiting values and the experimental $^3J_{C1,C6}$ values in **10**α, **10**β, **11**α, and **11**β against % $^4C_1$ form in solution were linear (Figure 3A). Very good agreement is observed between the limiting experimental and calculated $^3J_{C1,C6}$ in $^4C_1$ forms; values for the α-idohexopyranosyl ring are ~0.4 Hz smaller than for the β-idohexopyranosyl ring due to loss of the in-plane O1.[3,10] The difference between the limiting calculated $^3J_{C1,C6}$ values in

Scheme 7. Three Molecular Torsion Angles θ_1, θ_2, and ω Affect $^3J_{C1,C6}$ Values in Aldohexopyranosyl Rings

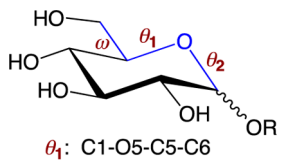

θ_1: C1-O5-C5-C6
θ_2: O1-C1-O5-C5
ω: O5-C5-C6-O6

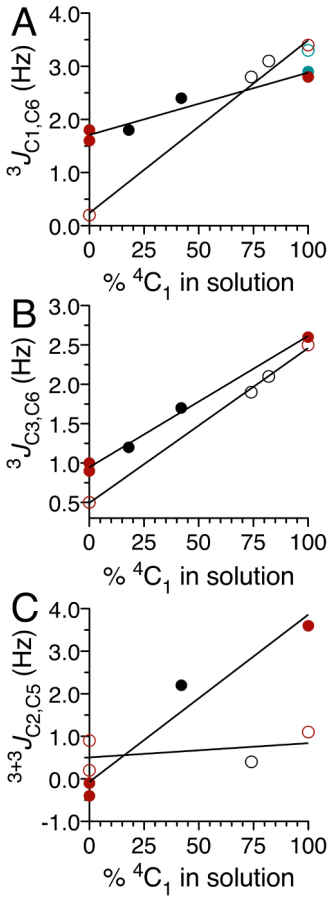

Figure 3. $^3J_{C1,C6}$ (A) and $^3J_{C3,C6}$ (B) as a function of % $^4C_1$ form in solutions of **10**α, **10**β, **11**α, and **11**β. (C) $^{3+3}J_{C2,C5}$ as a function of % $^4C_1$ form in solutions of **11**α and **11**β. Lines in each plot represent linear fits of the data. See Figure 1 for definitions of symbols.

DOI: 10.1021/acs.joc.6b02399
J. Org. Chem. 2017, 82, 1356−1370

the $^1C_4$ forms of both anomers is ~1.5 Hz, with the β-anomer showing the smaller coupling. This larger difference is attributed to the loss of the in-plane O1 and on structural factors associated with the C1−C6 diaxial interaction present in β-anomers.

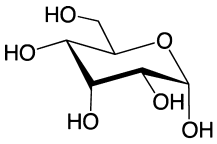

α-D-allopyranose **24**

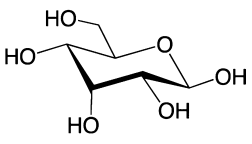

β-D-allopyranose **25**

$^3J_{C3,C6}$ values in aldohexopyranosyl rings show structural dependencies similar to $^3J_{C1,C6}$ but are also influenced by configuration at C4 and possibly by conformation of the C4−O4 bond.[9] Experimental $^3J_{C3,C6}$ values in **10**α/β and **11**α/β were interpreted using only limiting $^3J_{C3,C6}$ values obtained from DFT calculations (Table 2). The dynamic range for $^3J_{C3,C6}$ is small (Figure 3B), and structural perturbations could significantly affect the quality of the analysis. Nevertheless, the plot shown in Figure 3B is linear, indicating that the experimental $^3J_{C3,C6}$ values $^3J_{C3,C6}$ are consistent with the $^4C_1/^1C_4$ populations determined from the analysis of $^3J_{HH}$ values.

Two dual-pathway $^{13}C-^{13}C$ spin-couplings exist in aldopyranosyl rings, $^{3+3}J_{C1,C4}$ and $^{3+3}J_{C2,C5}$. In **11**α and **11**β, $^{3+3}J_{C1,C4}$ values are very similar (~1 Hz), but $^{3+3}J_{C2,C5}$ values differ significantly (2.2 Hz in **11**α; <0.7 Hz in **11**β) (Table 4). Calculated $^{3+3}J_{C2,C5}$ are ~0 Hz in **11**α in $^1C_4$ and 3.6 Hz in $^4C_1$ but very similar (~1 Hz) in both chair forms of **11**β. $^{3+3}J_{CC}$ values are determined by the algebraic sum of the individual couplings along both constituent pathways.[10] These pathways involve C−X−C−C torsion angles of ~±60° in the chair forms of aldopyranosyl rings (where X is either C or O). Both constituent couplings, being vicinal, are expected to have positive signs and thus add constructively. $^{3+3}J_{CC}$ values are determined by the number of oxygen atoms antiperiplanar to the coupled carbons; configuration at the coupled carbons does not appear to be a determinant.[10] For $^{3+3}J_{C2,C5}$, the relevant oxygens are O1, O3, and O4. When equatorial, these atoms are antiperiplanar to either C2 or C5 and reduce the coupling along the relevant pathway. Thus, **11**α contains no interactions in $^4C_1$ and three in $^1C_4$, while **11**β contains one interaction in $^4C_1$ and two in $^1C_4$. DFT-calculated $^{3+3}J_{C2,C5}$ values are consistent with these predictions, although the individual effects are not equivalent. For example, the conversion of **11**α to **11**β ($^4C_1$ forms) reduces $^{3+3}J_{C2,C5}$ by 2.4 Hz (addition of one *anti* interaction), whereas conversion of **11**β to **11**α ($^1C_4$ forms) reduces $^{3+3}J_{C2,C5}$ by ~0.7 Hz despite the same increase in *anti* interactions. These findings indicate that, in this case, the effect of configuration at the coupled carbons may not be negligible. Nonetheless, plots of the DFT-calculated limiting J-couplings and the experimental $^{3+3}J_{C2,C5}$ values in **11**α and **11**β against % $^4C_1$ form in solution are approximately linear (Figure 3C). The ~4 Hz dynamic range, which is comparable to those observed for single-pathway $^3J_{CC}$ values (Figure 3A,B), renders $^{3+3}J_{C2,C5}$ values potentially useful probes of pyranosyl ring conformation.

D. Behavior of $^3J_{H4,H5}$ Spin-Couplings in Idohexopyranosyl Rings. The above analyses of J_{HH}, J_{CH}, and J_{CC} values in D-idohexopyranosyl rings assumes that a two-site $^4C_1 \rightleftarrows {}^1C_4$ exchange model adequately describes ring conformational equilibria in solution. The linearities of the plots shown in Figures 1−3 support this contention. Other contributing conformations in solution are neglected despite calculations suggesting their presence, especially for the α-anomers (Scheme 4).[19] Prior interpretations of $^3J_{H4,H5}$ in **10**α suggested that skew forms such as $^0S_2$ may exist in solution.[18] This conclusion was based on the assumption that similar H4−C4−C5−H5 torsion angles in the $^4C_1$ (~−60°) and $^1C_4$ (~60°)

Scheme 8. Newman Projections for the C4−C5 Fragment in the $^4C_1$ (A) and $^1C_4$ (B) Conformers of 10α/β

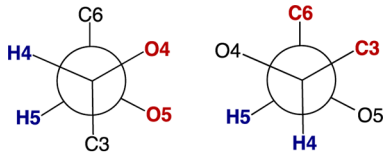

forms of **10**α (Scheme 8) give similar $^3J_{H4,H5}$ values and that $^3J_{H4,H5}$ values of 1.1−1.2 Hz observed in methyl α- (**26**) and β-D-galactopyranosides (**27**)[11,30] are reliable limiting values in $^4C_1$ forms. The larger experimental $^3J_{H4,H5}$ observed in **10**α (5.0 Hz) compared to **10**β (1.8 Hz) was interpreted as evidence of skewing in the C4−C5 fragment of the α-idopyranosyl ring toward nonchair forms containing smaller H4−C4−C5−H5 torsion angles.[18] However, a closer inspection of the C4−C5 Newman projection for **10**α (and **10**β) (Scheme 8) indicates that the H4−C4−C5−H5 torsion angles of −60° and +60° are not likely to yield similar $^3J_{H4,H5}$ values. In the $^4C_1$ forms of **10**α and **10**β, both H4 and H5 are antiperiplanar to an electronegative substituent (O5 and O4, respectively), but these arrangements are absent in the $^1C_4$ form. Electronegative substituents *anti* to coupled hydrogens truncate $^3J_{HCCH}$ values,[31] in this case appreciably since two *anti* interactions are involved. A considerably larger $^3J_{H4,H5}$ is therefore expected in the $^1C_4$ form than in the $^4C_1$ form. Consequently, the larger $^3J_{H4,H5}$ in **10**α relative to that in **10**β may be caused mostly by electronegative substituent effects and not by contributions from nonchair forms in solution.

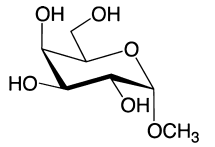

methyl α-D-galactopyranoside **26**

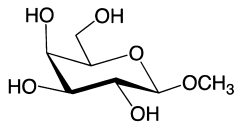

methyl β-D-galactopyranoside **27**

To test this possibility, experimental and DFT-calculated $^3J_{H4,H5}$ values in **10**α, **10**β, **11**α, and **11**β were plotted as a function of % $^4C_1$ form in solution (Figure 4). Limiting experimental $^3J_{H4,H5}$ values (100% $^4C_1$) were obtained from methyl α- (**26**) and β-D-galactopyranosides (**27**) (1.1 and 1.2 Hz).[11,30] Linear fitting of the data gave an extrapolated $^3J_{H4,H5}$ value of ~5.7 Hz in $^1C_4$ forms. Thus, the plot reveals a dynamic range of 4.5 Hz *despite the very similar H4−C4−C5−H5 torsion angles in both chair forms*. Limiting calculated $^3J_{H4,H5}$ values are shown in the plot but were not included in the fitting because they are may be influenced by exocyclic hydroxyl and hydroxymethyl conformations, factors not investigated in this work.

E. Anomalous Spin-Couplings in 11α. While the $^3J_{H4,H5}$ values in **10**α and **11**α do not provide experimental evidence for the presence of nonchair forms in solution (see above), five

DOI: 10.1021/acs.joc.6b02399
J. Org. Chem. 2017, 82, 1356−1370

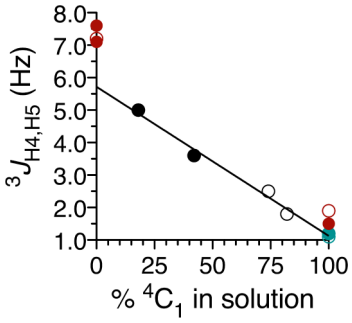

Figure 4. $^3J_{H4,H5}$ as a function of % $^4C_1$ form in solutions of **10**α, **10**β, **11**α, and **11**β. Lines were obtained from a linear fit of the experimental data only. See Figure 1 for definitions of symbols.

heteronuclear *J*-couplings, namely, $^2J_{C3,H4}$, $^3J_{C1,H5}$, $^3J_{C2,H4}$, $^3J_{C3,H5}$, and $^3J_{C6,H4}$, show behaviors suggestive of their presence. Most of these *J*-couplings report on structure in the C3−C6 regions of idohexopyranosyl rings.

The C1−O5−C5−H5 coupling pathway in methyl α-D-glucopyranoside **23** mimics that in the $^4C_1$ form of **11**α, whereas those in methyl β-D-glucopyranoside **17** and methyl β-D-arabinopyranoside **16** (involving $H5_{eq}$) mimic those in the $^4C_1$ and $^1C_4$ forms, respectively, of **11**β. When these data, the limiting DFT-calculated $^3J_{C1,H5}$ values, and the experimental $^3J_{C1,H5}$ values in **11**α and **11**β are plotted against the % $^4C_1$ form in solution (Figure 5A), good linearity is observed for **11**β but not for **11**α. The smaller than expected $^3J_{C1,H5}$ implicates the presence of nonchair contributors that contain relatively small C1−O5−C5−H5 torsion angles.

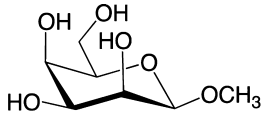

methyl β-D-talopyranoside **28**

$^3J_{C2,H4}$ in **11**α and **11**β exhibit behavior similar to that of $^3J_{C1,H5}$ (Figure 5B). Only one limiting experimental *J*-coupling is available in methyl β-talopyranoside **28** for $^4C_1$,[11] so the treatment relies heavily on limiting DFT-calculated values. The plot shows considerable scatter, but better agreement is observed for **11**β than for **11**α.

$^3J_{C3,H5}$ values depend strongly on ring conformation, with ∼1 Hz values observed in $^4C_1$ and ∼7 Hz values observed in $^1C_4$ forms (Figure 5C). The experimental coupling of 1.8 Hz in **11**β is reasonably well accommodated by a linear fit, but the 2.4 Hz value in **11**α is significantly smaller than predicted by the fit line.

DFT-calculated $^2J_{C3,H4}$ values are very similar in $^4C_1$ and $^1C_4$ forms of **11**α and **11**β, ranging from −4.0 to −4.5 Hz (Figure S4; see the Supporting Information). The experimental coupling of −4.3 Hz in **11**β is consistent with the fit line, but the −5.4 Hz value in **11**α is significantly more negative than predicted.

Finally, $^3J_{C6,H4}$ values are very different in the $^4C_1$ (∼1.5 Hz) and $^1C_4$ (∼5.5 Hz) forms of **11**α and **11**β (Figure S5; see the Supporting Information). The experimental coupling of 1.7 Hz in **11**β is consistent with the fit line, but the 2.2 Hz value in **11**α is considerably smaller than predicted.

Collectively, these results suggest that $^1C_4$-like forms may exist in solutions of **11**α, possibly coexisting with the two chair forms. However, a quantitative analysis of the complete ensemble of *J*-couplings in **11**α will be required to test conformational models more complex than the two-state $^4C_1$−$^1C_4$ model.

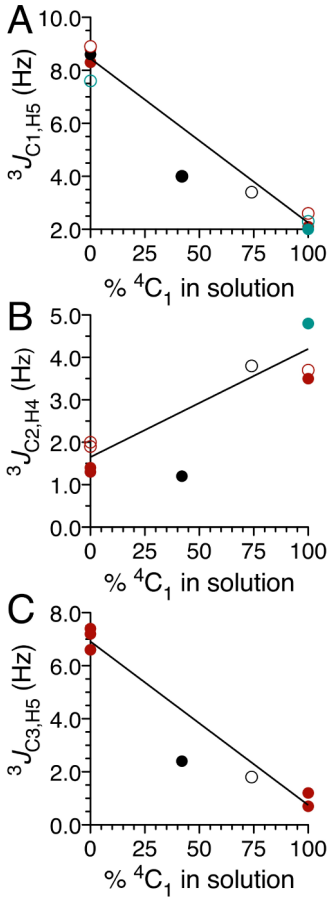

Figure 5. $^3J_{C1,H5}$ (A) and $^3J_{C2,H4}$ (B) as a function of % $^4C_1$ form in solutions of **11**α and **11**β. Lines represent linear fits of the limiting experimental and calculated data only. (C) $^3J_{C3,H5}$ as a function of % $^4C_1$ form in solutions of **11**α and **11**β. Line represents a linear fit of the limiting calculated and experimental data for **11**β. See Figure 1 for definitions of symbols.

F. Ring Conformation of Methyl α-L-[6-^{13}C]-Idopyranosiduronic Acid 12α. The effect of C6 oxidation on the conformational properties of **11**α was investigated to answer two questions: (1) Does C6 oxidation of **11**α to give methyl α-L-idopyranosiduronic acid **12**α affect pyranosyl ring conformational equilibria? (2) Does the ionization state of **12**α affect ring conformational equilibria? Obtaining reliable answers to both questions from *J*-couplings hinges on separating the intrinsic (i.e., conformation independent) effects of COOH ionization on *J*-couplings from those associated with a change in the ring conformational equilibrium. This separation was achieved using methyl α-D-[6-^{13}C]glucopyranosiduronic **29**α as the control. Nine *J*-couplings in **29**α were measured recently at pH 2 and 7 (Figure S6; see the Supporting Information) and found to change by 0.3 Hz or less in most cases.[32] The four intraring $^3J_{HH}$ values were essentially identical at pH 2 and pH 7, supporting the contention that ring conformation is unaltered upon COOH ionization (essentially $^4C_1$).

In contrast to **29**α, intraring $^3J_{HH}$ in [6-^{13}C]**12**α increase by 0.9−1.7 Hz as the solution pH increases from 1.7 to 7.0 (Figure 6) (Table S4, Supporting Information). J_{CH} and J_{CC} values

DOI: 10.1021/acs.joc.6b02399
J. Org. Chem. 2017, 82, 1356−1370

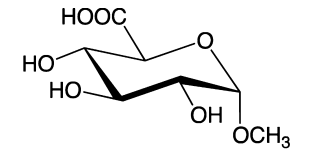

methyl α-D-glucopyranosiduronic acid **29**$^{p}\alpha$ ($^{4}C_1$ form)

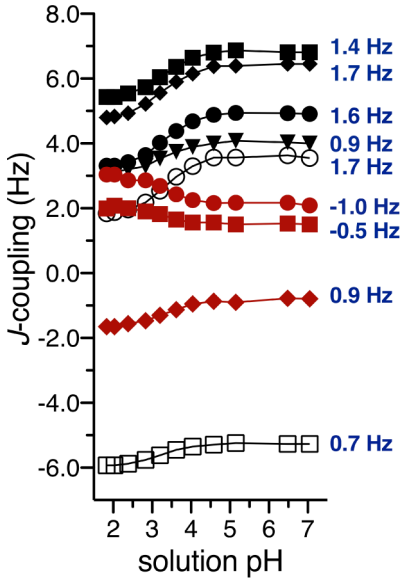

Figure 6. Effect of solution pH on J_{HH}, J_{CH}, and J_{CC} values in [6-^{13}C] **12**α. Values (shown in Hz) = $J_{pH\ 7.0} - J_{pH\ 1.8}$. Filled black circles, $^{3}J_{H1,H2}$; filled black squares, $^{3}J_{H2,H3}$; filled black diamonds, $^{3}J_{H3,H4}$; filled black inverted triangles, $^{3}J_{H4,H5}$; open black squares, $^{2}J_{C6,H5}$; open black circles, $^{3}J_{C6,H4}$; filled red diamonds; $^{2}J_{C6,C4}$; filled red circles, $^{3}J_{C6,C1}$; filled red squares, $^{3}J_{C6,C3}$.

involving the exocyclic C6 also depend on solution pH, with changes ranging from +1.7 Hz to −1.0 Hz (Figure 6). $^{3}J_{HH}$ values in the ionized form of **12**α, denoted **12**$^{i}\alpha$, are very similar to those found in **11**α, indicating similar ring conformational equilibria (~42% $^{4}C_1$ for **11**α; ~ 39% $^{1}C_4$ for **12**$^{i}\alpha$) (Scheme 9). The percentages of chair forms in solutions of the protonated form, denoted **12**$^{p}\alpha$, at pH 1.8 (based on $^{3}J_{H2,H3}$ and $^{3}J_{H3,H4}$ values; Table S4, Supporting Information) were calculated using eq 1: ~62% $^{1}C_4$, ~38% $^{4}C_1$ (Scheme 9). The percentage of $^{1}C_4$ form of **12**$^{p}\alpha$ is significantly higher than the ~42% $^{4}C_1$ form found for **11**α.

Scheme 9. Percentages of $^{4}C_1$ and $^{1}C_4$ Forms of 12α in Solution in Their Protonated and Deprotonated forms

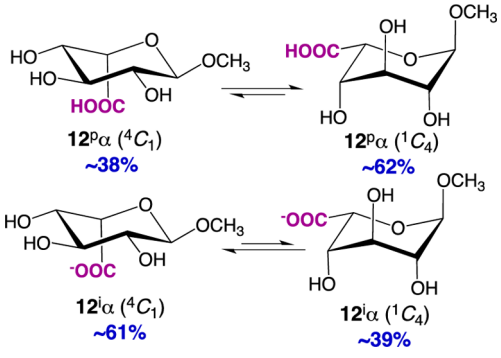

J_{CH} and J_{CC} values show a greater dependence on COOH ionization in **12**α than in **29**α (Figure 6; Figure S6, Supporting Information). For example, $^{3}J_{C6,H4}$ decreases by 0.2 Hz in **29**α and by 1.7 Hz in **12**α. If an intrinsic contribution of −0.2 Hz is assumed on the basis of the behavior of $^{3}J_{C6,H4}$ in **29**α, then ~1.9 Hz is attributed to a conformation effect in **12**α. This change is consistent with a higher percentage of $^{4}C_1$ form in **12**$^{i}\alpha$, since C6 and H4 are *gauche* in $^{1}C_4$ and antiperiplanar in $^{4}C_1$. Similar arguments pertain to $^{3}J_{C6,C1}$; in this case, the conformational effect contributes −0.7 Hz to $^{3}J_{C6,C1}$ upon COOH ionization. C1 and C6 are antiperiplanar in $^{1}C_4$ and *gauche* in $^{4}C_1$, with coupling decreasing as the percentage of $^{4}C_1$ form increases upon COOH ionization. However, $^{3}J_{C6,C3}$ exhibits little or no change upon COOH ionization, despite a change in the relative arrangement of the coupled atoms similar to that for $^{3}J_{C6,C1}$. Presumably, contributions from terminal (O3) and internal (O4) electronegative substituent effects negate the conformational contribution.

Changes in ring-conformational equilibria in **12**α upon COOH ionization also appear to be encoded in the pH dependencies of ^{1}H and ^{13}C chemical shifts. In **29**α, modest changes (<0.01 ppm) are observed for δ_{H2}, δ_{H3}, and δ_{OMe}, with H1 (−0.023 ppm), H4 (−0.055 ppm), and H5 (−0.250 ppm) showing progressively greater upfield shifts upon COOH ionization (Figure S7, Supporting Information). A much different pattern is observed for **12**α, with all but the OMe signals more shielded in the ionized state (Figure 7). The

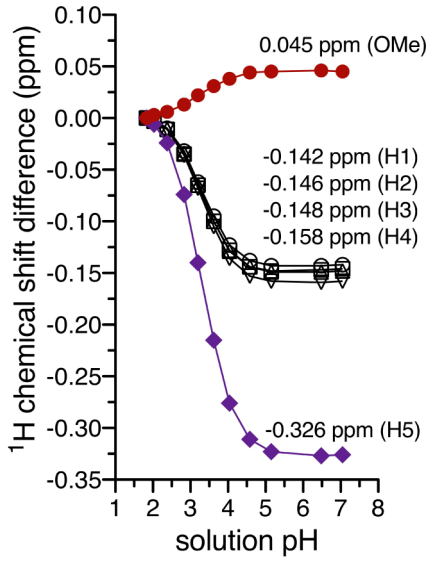

Figure 7. Effect of solution pH on ^{1}H chemical shifts in **12**α. Values in ppm are $\delta_{pH\ 7.0} - \delta_{pH\ 1.8}$.

differences are striking for the OMe, H1, H2, H3, and H4 signals, where conformational contributions exceed 0.1 ppm. The upfield shift in the H5 signal is also enhanced in **12**α upon ionization, with a conformational contribution of ~0.08 ppm (the intrinsic contribution of ~0.25 ppm dominates as expected, due to the proximity of H5 to the site of ionization). The enhanced upfield shifts upon COOH ionization in the H1, H2, H3, and H4 signals of **12**α are consistent with an increased percentage of $^{4}C_1$ form in solutions of **12**$^{i}\alpha$; changes from the equatorial hydrogen orientations in $^{1}C_4$ to the axial hydrogen orientations in $^{4}C_1$ are expected to cause upfield shifts in all four signals (see the Supporting Information).

DOI: 10.1021/acs.joc.6b02399
J. Org. Chem. 2017, 82, 1356−1370

^{13}C chemical shift dependencies on solution pH also differ significantly for **12**α and **29**α. In **29**α, all carbon signals except those for C1 and OMe shift downfield upon COOH ionization, with larger effects observed for C4, C5, and C6 (Figure S8, Supporting Information). These effects are intrinsic and scale inversely with proximity to the ionization site (closer nuclei show larger shifts). In contrast, the chemical shifts of carbon signals in **12**α do not exhibit this scaling, with the C2 and C3 signals showing changes equivalent to that observed for C5 (Figure 8). The downfield shifts of the C2 and C3 signals upon

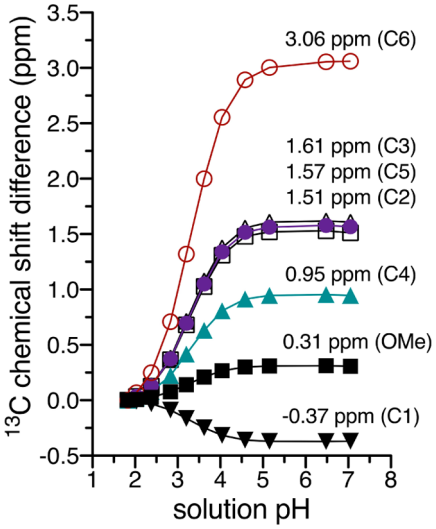

Figure 8. Effect of solution pH on ^{13}C chemical shifts in **12**α. Values in ppm are $\delta_{pH\ 7.0} - \delta_{pH\ 1.8}$.

COOH ionization are consistent with an increased percentage of $^4C_1$ form in solution; the C2−O2 and C3−O3 bonds are axial in the $^1C_4$ form and equatorial in the $^4C_1$ form, and conversion from axial to equatorial orientations is expected to be accompanied by downfield shifts (see the Supporting Information).

CONCLUSIONS

An analysis of intraring $^3J_{HH}$ values, assisted by theoretical $^3J_{HH}$ values obtained from DFT calculations, indicates that the $^4C_1$ and $^1C_4$ populations of α- and β-D-idopyranoses in aqueous solution differ, with ~18% $^4C_1$ found for **10**α and ~82% $^4C_1$ found for **10**β (for $^4C_1 \rightleftarrows {}^1C_4$ equilibria, $\Delta G^\circ_{10\alpha} = -0.9$ kcal/mol and $\Delta G^\circ_{10\beta} = +0.9$ kcal/mol at 25 °C) (Scheme 10). Conversion of D-idopyranoses to methyl D-idopyranosides shifts $^4C_1 \rightleftarrows {}^1C_4$ equilibria to ~42% $^4C_1$ for **11**α and ~74% $^4C_1$ for **11**β ($\Delta G^\circ_{11\alpha} = -0.2$ kcal/mol and $\Delta G^\circ_{11\beta} = +0.6$ kcal/mol) (Scheme 10). The percentage of $^4C_1$ in solution *increases* for **10**α and *decreases* for **10**β upon methyl glycosidation, and $\Delta\Delta G^\circ$ values, where $\Delta\Delta G^\circ = \Delta G^\circ_{\text{reducing sugar}} - \Delta G^\circ_{\text{glycoside}}$, are as follows: α-anomer, −0.7 kcal/mol; β-anomer, +0.3 kcal/mol. Methyl glycosidation stabilized idohexopyranosyl ring chair conformers containing an axial C1−O1 bond, presumably due to the stronger *endo*-anomeric effect in the glycosides.[21,22] The greater shift to an axial C1−O1 bond found in the $^4C_1$ form of **11**α (reflected in the larger value of $|\Delta\Delta G^\circ|$) is probably due in part to the Δ2 effect,[33−36] although the strength of the latter may be weakened by the axial C3−O3 bond, and different steric contributions in the glycoside and the reducing sugar (e.g., bulkier axial OCH_3 group) may play a role.[37] A

Scheme 10. Percentages of $^4C_1$ and $^1C_4$ Forms of 10α/β and 11α/β in Solution Based on NMR *J*-Coupling Analysis

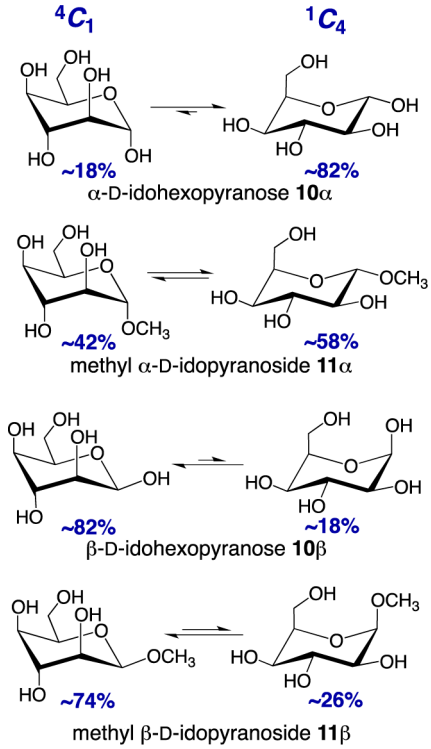

contribution from the Δ2 effect is absent in the conversion of $^4C_1$ forms to $^1C_4$ forms of **10**β and **11**β, thus causing the smaller shift. The $|\Delta\Delta G^\circ|$ value of 0.3 kcal/mol observed for the β-anomers is attributed mainly to the *endo*-anomeric effect in the $^1C_4$ conformer, although solvent effects may contribute. Assuming an equivalent *endo*-anomeric effect in the α-anomers of ~0.3 kcal/mol, the residual ~0.4 kcal/mol can be attributed to the Δ2 effect if solvent contributions are ignored. This behavior differs from that observed in conformationally rigid aldohexopyranosyl rings (*e.g.*, *gluco*, *manno*, *galacto*) where methyl glycosidation exerts little, if any, effect on $^4C_1 \rightleftarrows {}^1C_4$ equilibria. The unique properties of idohexopyranosyl rings are noteworthy given their occurrence in biologically important polysaccharides, commonly in the ionized form **12**$^i\alpha$ (*e.g.*, dermatan sulfate, heparin, heparin sulfate).[38] Ring substitution, and possibly solvent and other intermolecular interactions, can perturb idohexopyranosyl ring conformational equilibria (and presumably dynamics) significantly in solution, enabling different conformations in response to internal structural and/or external environmental cues. This property is presumably adaptive in biological contexts. Similar structure−function arguments have been made in prior reports.[38]

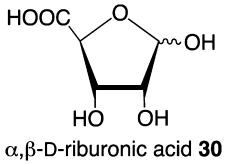

α,β-D-riburonic acid **30**

The conformational properties of uronic acid **12**α depend on the ionization state of its exocyclic COOH group. In this respect, **12**α behaves like conformationally flexible α,β-D-riburonic acid **30** whose intraring $^3J_{HH}$ values and by inference its ring conformation depend on the COOH ionization state

DOI: 10.1021/acs.joc.6b02399
J. Org. Chem. 2017, 82, 1356−1370

(as does its anomeric ratio).[39] The behavior of **12**α differs from that of **29**α, which highly prefers the $^4C_1$ ring conformation in aqueous solution in both its protonated and ionized states.[32] The $^4C_1 \rightleftarrows {}^1C_4$ equilibrium for **12**$^i\alpha$ more closely resembles that of **11**α than does **12**$^p\alpha$; the chair form bearing four equatorial exocyclic C−O bonds is preferred (~58% $^1C_4$ for **11**α; ~ 61% $^4C_1$ for **12**$^i\alpha$). Aqueous solutions of **12**$^p\alpha$ contain significantly more $^1C_4$ form than do those of **12**$^i\alpha$; that is, **12**$^p\alpha$ prefers a ring conformation in which the C5−C6 bond is equatorial and the C1−O1 bond is axial. Whether these two factors are reinforcing is unclear. The COOH group may strengthen the *endo*-anomeric effect in **12**$^p\alpha$ relative to the COO^- group in **12**$^i\alpha$ or the CH_2OH group in **11**α, thus shifting the $^4C_1 \rightleftarrows {}^1C_4$ equilibrium toward the $^1C_4$ form. In contrast, the COO^- group in **12**$^i\alpha$ appears to be structurally equivalent to the CH_2OH group in **11**α with regard to influencing $^4C_1 \rightleftarrows {}^1C_4$ equilibria. Differential solvation and/or differential nonbonded interactions may also play a role in determining $^4C_1 \rightleftarrows {}^1C_4$ chair equilibria in **12**$^p\alpha$ and **12**$^i\alpha$. However, regardless of the origin of the pH effect, the results show that the $^4C_1 \rightleftarrows {}^1C_4$ equilibrium for **12**α depends on the COOH ionization state, and this property could play a pivotal role in determining its biological properties and functions. Within the series **10**α, **11**α, **12**$^p\alpha$, and **12**$^i\alpha$, the percentage of chair forms containing four axial exocyclic C−O bonds ($^4C_1$ in the D-series, $^1C_4$ in the L-series) increases as follows: 18% (**10**α) < 39% (**12**$^i\alpha$) ≈ 42% (**11**α) < 62% (**12**$^p\alpha$).

A two-state $^4C_1 \rightleftarrows {}^1C_4$ conformational model was used in this study to interpret *J*-couplings and chemical shifts in idohexopyranosyl rings. The reported percentages of $^4C_1$ and $^1C_4$ forms, however, may not strictly pertain to only two discrete chair forms, but rather to $^4C_1$-like and $^1C_4$-like forms, implying ranges of related conformers that may include the two idealized chairs. For **10**β and **11**β, the two-state model fits all of the available *J*-coupling data satisfactorily; contributions from nonchair forms in solution appear negligible. For **10**α and **11**α, however, most of the available *J*-couplings are consistent with the two-state model, and several are not. The former group reports mainly on structure in the O5−C1−C2−C3 fragment of the pyranosyl ring, while the latter group reports mainly on the C3−C4−C5−O5 fragment. The graphical treatments described herein point to possible ring distortions in the latter fragment in the α-anomers. Few *experimental* data are currently available that support a more complex conformational model for **10**α and **11**α. A comprehensive quantitative treatment of complete ensembles of *J*-couplings in **10**α and **11**α may enable unbiased testing of a wider range of conformational models to determine which best fit the data. A similar approach has been taken recently to interpret redundant trans-*O*-glycoside *J*-couplings in oligosaccharides in terms of ϕ and ψ rotamer populations (Scheme 1).[40]

The $^4C_1$−$^1C_4$ equilibria for **10**α, **10**β, **11**α, and **11**β in solution (Scheme 10) were initially determined by analyzing experimental $^3J_{HH}$ values using DFT-calculated limiting $^3J_{HH}$ values and eq 1. J_{CH} and J_{CC} values were then tested for their consistency with the derived chair equilibria using both experimental and DFT-calculated limiting *J*-couplings. In addition to testing the derived chair equilibria, this approach also revealed the sensitivities of specific J_{CH} and J_{CC} values to aldohexopyranosyl ring conformation. The findings support the contention that modern experimental conformational analyses of aldohexopyranosyl rings need not depend solely on relatively few intraring $^3J_{HH}$ values, but rather on a larger ensemble that includes J_{CH} and J_{CC} values. In some experimental cases where reliable $^3J_{HH}$ values may not be accessible, J_{CH} and J_{CC} values are viable alternatives for the reliable assignment of ring conformation, even in the presence of conformational averaging.

This work provides new data to gauge the accuracy of *J*-couplings calculated by DFT. In most cases, the calculated *J*-couplings were in good agreement with experimental measurements for coupling pathways involving two or three bonds. Larger absolute errors were observed for one-bond $^1J_{CH}$ and $^1J_{CC}$ values, which is not surprising given the critical role that C−O bond conformation plays in dictating their magnitudes[4,10] and the inability to accurately replicate these behaviors in a computationally practical manner at the present time.

A key motivation of this work was to determine NMR-derived $^4C_1 \rightleftarrows {}^1C_4$ equilibria for **10**α, **10**β, **11**α, **11**β, **12**$^p\alpha$, and **12**$^i\alpha$ for comparison to those predicted by molecular dynamics (MD) simulations and other computational methods. Replication of the experiment-based equilibria in MD simulations would serve as a means to confirm the reliability of the MD methodology. A similar approach to validating MD results has been taken recently in conformational analyses of *O*-glycosidic linkages in oligosaccharides and will be discussed in an upcoming report.[41]

Recent aqueous MD simulations of the L-enantiomers of **11**α and **11**β indicate that the α-L-pyranoside highly favors the $^1C_4$ form (~85%) (structurally equivalent to the $^4C_1$ form of **11**α), while the β-L-pyranoside almost exclusively prefers the $^1C_4$ form (99.5%).[14] These preferences are inconsistent with those found in this study. For **11**β, the MD results predict almost 100% $^4C_1$ form (D-isomer), but *J*-coupling analysis indicates ~74%. For **11**α, 85% $^4C_1$ is predicted by MD, but 42% is found from *J*-coupling analysis. In the present case, it is unlikely that the discrepancies are caused by insufficient simulation time (10 μs). Solvation factors, specifically H-bonding interactions either with solvent water or between hydroxyl groups on the pyranosyl ring, might be responsible, although inaccurate treatments of overlapping stereoelectronic effects (*endo*-anomeric effect; Δ2 effect) may also contribute.

Recent 10 ns MD simulations of **12**$^i\alpha$ by Oborsky and coworkers[42] gave relative populations of $^4C_1$, $^1C_4$, and $^2S_0$ conformers that depended on the type of van der Waals and electrostatic scaling employed in the simulations. The following percentages were obtained from five different scaling schemes: (a) 100% $^4C_1$; (b) 83% $^1C_4$/17% $^4C_1$; (c) 85% $^1C_4$/14% $^4C_1$/1% $^2S_0$; (d) 73% $^1C_4$/25% $^4C_1$/2% $^2S_0$; (e) 70% $^1C_4$/22% $^4C_1$/5% $^2S_0$/3% other. The experimental $^4C_1 \rightleftarrows {}^1C_4$ equilibrium determined for **12**$^i\alpha$ in the present work (~61% $^4C_1$ and 39% $^1C_4$; Scheme 9) is in closest agreement with (e) in which scaling factors of 1.0 and 3.0 were employed for the Coulombic and van der Waals interactions, respectively.

MD results for **12**α reported by Babin and Sagui[43] are difficult to interpret because the ionization state used in the simulations was not identified, although it appears to be **12**$^p\alpha$. ΔG° for the $^1C_4 \rightleftarrows {}^4C_1$ equilibrium was reported to be +0.71 kcal/mol, translating into 77% $^1C_4$ and 23% $^4C_1$ at 298 K. Experimental data reported herein gave 62% $^1C_4$ and 38% $^4C_1$ forms in aqueous solutions of **12**$^p\alpha$ (Scheme 9), in reasonable agreement with the MD findings. Interestingly, the authors report a discrepancy between $^3J_{HH}$ values back-calculated from their MD results ($^3J_{H1,H2}$ = 3.66 Hz; $^3J_{H2,H3}$ = 3.69 Hz; $^3J_{H3,H4}$ = 3.86 Hz; $^3J_{H4,H5}$ = 3.54 Hz) and prior experimental $^3J_{HH}$ data,[44] the latter indicating a preference for the $^4C_1$ conformer.

DOI: 10.1021/acs.joc.6b02399
J. Org. Chem. 2017, 82, 1356−1370

However, the latter experimental $^3J_{HH}$ values more closely resemble those measured in **12**$^i\alpha$ than in **12**$^p\alpha$ ($^3J_{H1,H2}$ = 4.9 Hz; $^3J_{H2,H3}$ = 6.6 Hz; $^3J_{H3,H4}$ = 6.0 Hz; $^3J_{H4,H5}$ = 4.0 Hz) (Table S4, Supporting Information), thus explaining the preference for the $^4C_1$ conformer (Scheme 9). A different conclusion about the level of agreement between the MD and experimental *J*-couplings might have been reached had the effect of COOH ionization on the $^4C_1 \rightleftarrows {}^1C_4$ equilibrium been taken into account in the simulations.

Recent 10 μs aqueous MD simulations of **12**$^i\alpha$ by Sattelle and co-workers[45] indicate that $^4C_1$ and skew-boat (mainly ^2S_O) conformers are 0.9 and 2.6 kcal/mol *higher* in energy, respectively, than the $^1C_4$ form, translating into 18% $^4C_1$ and 82% $^1C_4$ in solutions of **12**$^i\alpha$ at 25 °C. A much higher percentage of the $^4C_1$ form (~61%) was found in this work (Scheme 9).

In summary, aqueous MD simulations to date predict widely different $^4C_1 \rightleftarrows {}^1C_4$ equilibria for **12**α and do not address the effect of COOH ionization on the equilibrium. MD-predicted percentages of the $^4C_1$ form in aqueous solutions of **12**$^i\alpha$ vary from 18% to 100% depending on the parameters used in the simulations. This range brackets the percentages obtained in the present work (~38% for **12**$^p\alpha$ and ~61% for **12**$^i\alpha$).

In addition to NMR *J*-couplings, some ^{1}H and ^{13}C chemical shifts depend on the $^4C_1 \rightleftarrows {}^1C_4$ conformational equilibria of idohexopyranosyl rings. C5 chemical shifts differ considerably in the $^4C_1$ and $^1C_4$ forms, as do δ_{H2}, δ_{H3}, δ_{H4}, and δ_{H5}, with δ_{H2} and δ_{H3} showing particular sensitivity. In contrast to *J*-couplings whose magnitudes are determined largely by local bonding environments, chemical shifts, especially for the solvent-exposed ^{1}H nuclei, may be significantly affected by environmental factors, making their use potentially prone to misinterpretation. Nevertheless, δ_{C5}, δ_{H2}, δ_{H3}, δ_{H4}, and δ_{H5} may prove to be valuable probes of idohexopyranosyl ring conformational equilibria for molecules free in solution and in receptor-bound states.

EXPERIMENTAL SECTION

Synthesis of Methyl α- and β-D-[^{13}C]Idopyranosides 11α and 11β.[46] D-[1-^{13}C]Idose was prepared by cyanohydrin reduction using D-xylose and K^{13}CN as the primary reactants.[47,48] D-[2-^{13}C]Idose and D-[3-^{13}C]idose were prepared in a similar fashion using D-[1-^{13}C]-xylose and D-[2-^{13}C]xylose, respectively, as the aldopentose reactants. The C2-epimeric products, D-[^{13}C]idose and D-[^{13}C]gulose, were separated by chromatography on a column (3 cm × 100 cm) containing Dowex 50 × 8 (200–400 mesh) ion-exchange resin in the Ca^{2+} form[49] using distilled water as the eluent; D-idose eluted first, followed by D-gulose. Some peak overlap was observed, but careful pooling of fractions gave pure samples of labeled D-idose.

L-[6-^{13}C]Idose was prepared by the addition of K^{13}CN to 1,2-isopropylidene-α-D-*xylo*-pentodialdo-1,4-furanose.[50]

The D-[^{13}C]idoses were converted into methyl D-[^{13}C]-idopyranosides by Fischer glycosidation.[11] After the reaction was complete (~2 h), the solution was cooled, the resin catalyst was removed by vacuum filtration, and the methanolic solution was concentrated at 30 °C in vacuo to a syrup. ^{13}C NMR of the syrup in ^2H_2O indicated that idofuranosides, idopyranosides, and the 1,6-anhydro derivative were present. The syrup was dissolved in a minimal volume of distilled water, and the solution was applied to a column (2.5 cm × 100 cm) containing Dowex 1 × 8 (200–400 mesh) ion-exchange resin in the OH^- form.[51] The column was eluted with distilled, decarbonated water, and fractions were assayed with phenol–sulfuric acid[52] to locate the pyranosides. Careful pooling of fractions gave >95% pure methyl α-D-[^{13}C]idopyranoside (**11**α) and methyl β-D-[^{13}C]idopyranoside (**11**β) as determined by ^{1}H NMR. The anomers were assigned on the basis of characteristic anomeric ^{1}H signal multiplicities reported for the α- and β-D-idopyranoses[18] and on reported ^{13}C NMR data for **11**α.[53]

Synthesis of Methyl α-L-[6-^{13}C]Idopyranosiduronic Acid 12α.[46] L-[6-^{13}C]Idose[50] (500 mg, 2.78 mmol) was dissolved in anhydrous methanol (30 mL), dry Dowex 50 W × 8 (200–400 mesh) (H^+) ion-exchange resin (0.5 g) was added, and the suspension was refluxed for 3 h. After cooling and filtration to remove the resin, the filtrate was concentrated to dryness at 30 °C in vacuo, the residue was dissolved in a minimum volume of distilled water, and the solution was applied to a column (2.5 cm × 110 cm) containing Dowex 50 × 8 (200–400 mesh) ion-exchange resin in the Ca^{2+} form.[49] The column was eluted with distilled, decarbonated water (1.0 mL/min), and fractions (10 mL) were collected and assayed with phenol–sulfuric acid.[52] Fractions containing the idopyranosides were pooled and evaporated to dryness at 30 °C in vacuo to give methyl α-L-[6-^{13}C]idopyranoside (fractions 29–31) (80 mg, 0.41 mmol) and methyl β-L-[6-^{13}C]idopyranoside (fractions 35–37) (90 mg, 0.46 mmol). The anomers were assigned on the basis of characteristic anomeric ^{1}H signal multiplicities reported for the α- and β-D-idopyranoses[18] and on reported ^{13}C NMR data for **11**α.[53]

Methyl α-L-[6-^{13}C]idopyranoside (80 mg, 0.41 mmol) was dissolved in distilled water (20 mL, pH ~7.5), and sodium bicarbonate (20 mg) was added to adjust the solution pH to 8.4. To this solution was added 5% platinum on activated carbon catalyst (Pt/C; 15 mg, prereduced under H_2).[39,46] The reaction flask was evacuated and filled several times with O_2 and then partially immersed in an oil bath at 50 °C. The mixture was stirred for 6 h, during which time the solution pH was maintained above 7 with occasional additions of solid sodium bicarbonate. After catalyst removal by vacuum filtration, the reaction mixture was applied to a column (2.5 cm × 25 cm) of DEAE-Sephadex A-25 anion-exchange resin in the bicarbonate form, and the column was eluted with a 2 L linear gradient (0–0.07 M) of sodium bicarbonate at a flow rate of 1.0 mL/min.[39] Fractions (15 mL) were collected and assayed for uronic acid by TLC (silica gel; spots detected by charring after spraying with 1% (w/v) $CeSO_4$–2.5% (*w*/*v*) $(NH_4)_6Mo_7O_{24}$–10% aq H_2SO_4 reagent[54]). Fractions 49–53 containing **12**α were pooled and concentrated at 30 °C in vacuo to ~10 mL. This solution was treated batchwise with excess Dowex HCR-W2 (H^+) ion-exchange resin, the resin was removed by filtration, and the filtrate was frozen and lyophilized. The yield of **12**α from the Pt/O_2 oxidation reaction was ~40% (35 mg, 0.17 mmol) based on the weight of the lyophilized product. The ^{1}H and ^{13}C NMR spectra of **12**α compared favorably with those reported previously.[46]

NMR Spectroscopy. High-resolution ^{1}H NMR spectra of ^{13}C-labeled **11**α and **11**β in ^2H_2O (~10 mM in glycoside) were obtained at 750 MHz and 25 °C. Spectra were collected with 2000–3000 Hz sweep widths and 32 K points, and FIDs were zero-filled before processing with resolution enhancement to improve spectral resolution. Since ^{1}H spectra of **11**α and **11**β were not first-order at 750 MHz, spectra were simulated using the MacNUTs program[55] to extract accurate chemical shifts and *J*-couplings. Reported ^{1}H chemical shifts are accurate to ±0.002 ppm, and reported J_{HH} and J_{CH} values are accurate to ±0.2 Hz, unless otherwise indicated. ^{1}H Chemical shifts were referenced to the internal residual HOD signal at 4.800 ppm.

^{13}C{^{1}H} NMR spectra of **11**α and **11**β were obtained at 150 MHz in ^2H_2O (~30 mM in glycoside) and 21 °C. Spectra were collected with 8500 Hz sweep widths and 128 K points, and FIDs were zero-filled before processing with resolution enhancement to improve spectral resolution. Reported ^{13}C chemical shifts are accurate to ±0.1 ppm, and reported J_{CC} are accurate to ±0.1 Hz unless otherwise indicated. ^{13}C Chemical shifts were referenced externally to the C1 signal of α-D-[1-^{13}C]mannopyranose (95.50 ppm).[8]

For ^{1}H and ^{13}C NMR studies of **12**α, aqueous solutions were prepared at different solution pD (pH meter reading on the ^2H_2O solution after calibration of a microelectrode with standard buffers) by dissolving samples in ^2H_2O and adjusting the solution pD with NaOD or with batchwise addition of Dowex HCR-W2 (H^+) (16–40 mesh) ion-exchange resin. Final solutions were ~150 mM in **12**α. High-resolution 1D ^{1}H and ^{13}C{^{1}H} NMR spectra were obtained at 22 °C

DOI: 10.1021/acs.joc.6b02399
J. Org. Chem. 2017, 82, 1356–1370

on a 600 MHz FT-NMR spectrometer equipped with a 5 mm $^{1}H-^{19}F/^{15}N-^{31}P$ AutoX dual broadband probe. 600 MHz ^{1}H NMR spectra were collected with a 2100 Hz spectral window and a ~4.0 s recycle time, and reported ^{1}H chemical shifts and *J*-couplings (J_{HH} and J_{CH}) are accurate to ±0.001 ppm and ±0.1 Hz unless otherwise stated. $^{13}C\{^{1}H\}$ NMR spectra (150 MHz) were collected with an ~28000 Hz spectral window and a ~5.5 s recycle time. FIDs were zero-filled to give final digital resolutions of <0.05 Hz/point, and FIDs were processed with resolution enhancement (Gaussian or sine-bell functions) to improve spectral resolution and facilitate the measurement of smaller *J*-couplings. The degree of enhancement was chosen empirically based on the observed effects on line shape and spectral S/N. Reported ^{13}C chemical shifts and *J*-couplings (J_{CC}) are accurate to ±0.01 ppm and ±0.1 Hz unless otherwise stated. ^{1}H and ^{13}C Chemical shifts were referenced externally to sodium 4,4-dimethyl-4-silapentane-1-sulfonate (DSS).

Calculations. *Geometric Optimization of Model Structures.* Two series of density functional theory (DFT) calculations were conducted within *Gaussian*09[56] using the B3LYP functional[57] and 6-31G* basis set[58] for geometric optimization. DFT calculations included the effects of solvent water, which were treated using the self-consistent reaction field (SCRF)[59] and the integral equation formalism (polarizable continuum) model (IEFPCM).[60] In series 1, structures $\mathbf{11}\alpha_1^{C1}$, $\mathbf{11}\alpha_2^{C1}$, $\mathbf{11}\beta_1^{C1}$, and $\mathbf{11}\beta_2^{C1}$ (Scheme 5) were investigated (note that the superscript "C" denotes a DFT calculated (*in silico*) structure (to be distinguished from chemical compounds **11**α and **11**β), the superscripts "1" and "2" denote the series, and the subscripts "1" and "2" denote $^{4}C_1$ and $^{1}C_4$ forms, respectively). In these optimizations, five exocyclic C−O or C−C bond torsion angles were fixed at the values shown in Scheme 5. In series 2, three C−O bonds in $\mathbf{11}\alpha_2^{C1}$ and $\mathbf{11}\beta_2^{C1}$ were rotated to the fixed values shown in Scheme 5, and the resulting structures, denoted $\mathbf{11}\alpha_2^{C2}$ and $\mathbf{11}\beta_2^{C2}$, were reoptimized. In series 1 and 2, the C2−C1−O1−CH_3 torsion angles were set initially at 180° and allowed to optimize (Scheme 5). Values of this torsion angle in the optimized structures were as follows: $\mathbf{11}\alpha_1^{C1}$(−173.3°), $\mathbf{11}\alpha_2^{C1}$ (−167.7°), $\mathbf{11}\alpha_2^{C2}$ (−168.0°), $\mathbf{11}\beta_1^{C1}$ (168.0°), $\mathbf{11}\beta_2^{C1}$ (170.1°), $\mathbf{11}\beta_2^{C2}$ (168.0°).

DFT Calculations of NMR Spin-Coupling Constants in Model Structures. J_{HH}, J_{CH}, and J_{CC} spin-coupling constants were calculated in $\mathbf{11}\alpha_1^{C1}$, $\mathbf{11}\alpha_2^{C1}$, $\mathbf{11}\beta_1^{C1}$, $\mathbf{11}\beta_2^{C1}$, $\mathbf{11}\alpha_2^{C2}$, and $\mathbf{11}\beta_2^{C2}$ using *Gaussian*09[56] and DFT (B3LYP).[57] The Fermi contact,[61−63] diamagnetic and paramagnetic spin−orbit, and spin-dipole terms[61] were recovered using a specially designed basis set, [5s2p1d|3s1p],[4] and raw (unscaled) calculated couplings are reported; these values have an average estimated error of ±5% based on prior work.[4] *J*-coupling calculations included the effects of solvent water and were treated using the self-consistent reaction field (SCRF)[59] and the integral equation formalism (polarizable continuum) model (IEFPCM)[60] as implemented in *Gaussian*09.

■ ASSOCIATED CONTENT

Supporting Information

The Supporting Information is available free of charge on the ACS Publications website at DOI: 10.1021/acs.joc.6b02399.

Scheme S1, Figures S1−S8, Tables S1−S4, analysis of ^{13}C and ^{1}H chemical shifts in idohexopyranosyl rings; DFT calculations of δ_{C5} in idohexopyranosyl rings; hydroxymethyl group conformation in idohexopyranosyl rings; assumptions made in assigning hydroxymethyl group conformation in idohexopyranosyl rings; Cartesian coordinates for $\mathbf{11}\alpha_1^{C1}$, $\mathbf{11}\alpha_2^{C1}$, $\mathbf{11}\beta_1^{C1}$, $\mathbf{11}\beta_2^{C1}$, $\mathbf{11}\alpha_2^{C2}$ and $\mathbf{11}\beta_2^{C2}$; complete ref 52 (PDF)

■ AUTHOR INFORMATION

Corresponding Author

*E-mail: aseriann@nd.edu.

ORCID

Anthony S. Serianni: 0000-0001-6114-1446

Notes

The authors declare no competing financial interest.

■ ACKNOWLEDGMENTS

We thank Omicron Biochemicals, Inc., of South Bend, IN, for several ^{13}C-labeled monosaccharides used in this study. This work was supported by grants from the National Institutes of Health (GM59239) and the National Science Foundation (CHE 1402744) (to A.S.). The Notre Dame Radiation Laboratory is supported by the U.S. Department of Energy Office of Science, Office of Basic Energy Sciences, under Award Number DE-FC02-04ER15533. This is Document No. NDRL-5041 from the Notre Dame Radiation Laboratory. We also thank Dr. Allen Oliver for assistance in calculating Cremer−Pople parameters given in Table S1 of the Supporting Information.

■ REFERENCES

(1) Varki, A. *Glycobiology* **1993**, *3*, 97−130.
(2) Taylor, M. E.; Drickamer, K. *Introduction to Glycobiology*, 3rd ed., Oxford University Press, 2011.
(3) Bose, B.; Zhao, S.; Stenutz, R.; Cloran, F.; Bondo, P. B.; Bondo, G.; Hertz, B.; Carmichael, I.; Serianni, A. S. *J. Am. Chem. Soc.* **1998**, *120*, 11158−11173.
(4) Stenutz, R.; Carmichael, I.; Widmalm, G.; Serianni, A. S. *J. Org. Chem.* **2002**, *67*, 949−958.
(5) Ionescu, A. R.; Bérces, A.; Zgierski, M. Z.; Whitfield, D. M.; Nukada, T. *J. Phys. Chem. A* **2005**, *109*, 8096−8105.
(6) Cloran, F.; Zhu, Y.; Osborn, J.; Carmichael, I.; Serianni, A. S. *J. Am. Chem. Soc.* **2000**, *122*, 6435−6448.
(7) Voet, D.; Voet, J. G. *Biochemistry*, 4th ed.; John Wiley & Sons, 2011; p 360.
(8) King-Morris, M. J.; Serianni, A. S. *J. Am. Chem. Soc.* **1987**, *109*, 3501−3508.
(9) Wu, J.; Bondo, P. B.; Vuorinen, T.; Serianni, A. S. *J. Am. Chem. Soc.* **1992**, *114*, 3499−3503.
(10) Bose-Basu, B.; Klepach, T.; Bondo, G.; Bondo, P. B.; Zhang, W.; Carmichael, I.; Serianni, A. S. *J. Org. Chem.* **2007**, *72*, 7511−7522.
(11) Podlasek, C. A.; Wu, J.; Stripe, W. A.; Bondo, P. B.; Serianni, A. S. *J. Am. Chem. Soc.* **1995**, *117*, 8635−8644.
(12) Collins, P.; Ferrier, R. *Monosaccharides − Their Chemistry and Their Roles in Natural Products*; John Wiley & Sons: Chichester, 1995; p 534.
(13) Sattelle, B. M.; Almond, A. *Glycobiology* **2011**, *21*, 1651−1662.
(14) Sattelle, B. M.; Bose-Basu, B.; Tessier, M.; Woods, R. J.; Serianni, A. S.; Almond, A. *J. Phys. Chem. B* **2012**, *116*, 6380−6386.
(15) Jardetzky, O. *Biochim. Biophys. Acta, Protein Struct.* **1980**, *621*, 227−232.
(16) Canales, A.; Jiménez-Barbero, J.; Martin-Pastor, M. *Magn. Reson. Chem.* **2012**, *50*, S80−85.
(17) Bell, N. G. A.; Rigg, G.; Masters, S.; Bella, J.; Uhrín, D. *Phys. Chem. Chem. Phys.* **2013**, *15*, 18223−18234.
(18) Snyder, J. R.; Serianni, A. S. *J. Org. Chem.* **1986**, *51*, 2694−2702.
(19) Kurihara, Y.; Ueda, K. *Carbohydr. Res.* **2006**, *341*, 2565−2574.
(20) French, A. D.; Brady, J. W. Computer Modeling of Carbohydrates. In *Computer Modeling of Carbohydrate Molecules*; French, A. D., Brady, J. W., Eds.; ACS Symposium Series 430; American Chemical Society, Washington, DC, 1990; p 11.
(21) Lemieux, R. U.; Kullnig, R. K.; Bernstein, H. J.; Schneider, W. G. *J. Am. Chem. Soc.* **1958**, *80*, 6098−6105.
(22) Praly, J.-P.; Lemieux, R. U. *Can. J. Chem.* **1987**, *65*, 213−223.
(23) Serianni, A. S.; Kline, P. C.; Snyder, J. R. *J. Am. Chem. Soc.* **1990**, *112*, 5886−5887.
(24) Snyder, J. R.; Johnston, E. R.; Serianni, A. S. *J. Am. Chem. Soc.* **1989**, *111*, 2681−2687.

DOI: 10.1021/acs.joc.6b02399
J. Org. Chem. 2017, 82, 1356−1370

(25) Cloran, F.; Carmichael, I.; Serianni, A. S. *J. Phys. Chem. A* **1999**, *103*, 3783−3795.
(26) Church, T.; Carmichael, I.; Serianni, A. S. *Carbohydr. Res.* **1996**, *280*, 177−186.
(27) Hadad, M. J.; Zhang, W.; Turney, T.; Sernau, L.; Wang, X.; Woods, R. J.; Incandela, A.; Surjancev, I.; Wang, A.; Yoon, M.; Coscia, A.; Euell, C.; Meredith, R.; Carmichael, I.; Serianni, A. S. In: *NMR in Glycoscience and Glycotechnology*; Kato, K., Peters, T., Eds.; Royal Society of Chemistry, 2017, in press.
(28) Serianni, A. S.; Bondo, P. B.; Zajicek, J. *J. Magn. Reson., Ser. B* **1996**, *112*, 69−74.
(29) Zhao, S.; Bondo, G.; Zajicek, J.; Serianni, A. S. *Carbohydr. Res.* **1998**, *309*, 145−152.
(30) Thibaudeau, C.; Stenutz, R.; Hertz, B.; Klepach, T.; Zhao, S.; Wu, Q.; Carmichael, I.; Serianni, A. S. *J. Am. Chem. Soc.* **2004**, *126*, 15668−15685.
(31) Günther, H. *NMR Spectroscopy*, 2nd ed.; John Wiley & Sons: New York, 1995; pp 119−121.
(32) Zhang, W.; Hu, X.; Carmichael, I.; Serianni, A. S. *J. Org. Chem.* **2012**, *77*, 9521−9534.
(33) Reeves, R. E. *J. Am. Chem. Soc.* **1950**, *72*, 1499−1506.
(34) Reeves, R. E. *Annu. Rev. Biochem.* **1958**, *27*, 15−34.
(35) Angyal, S. J. *Aust. J. Chem.* **1968**, *21*, 2737−2746.
(36) Durette, P. L.; Horton, D. *Adv. Carbohydr. Chem.* **1971**, *26*, 49−125.
(37) Collins, P.; Ferrier, R. *Monosaccharides*; John Wiley & Sons: New York, 1995; p 31.
(38) Mulloy, B.; Forster, M. J. *Glycobiology* **2000**, *10*, 1147−1156.
(39) Wu, J.; Serianni, A. S. *Carbohydr. Res.* **1991**, *210*, 51−70.
(40) Sernau, L.; Klepach, T.; Serianni, A. S. Experimental Validation of Saccharide MD Simulations: Quantitative Treatment of NMR J-Coupling Ensembles. *13th Tetrahedron Symposium, Asia Edition*, Nov 27−30, 2012.
(41) Zhang, W.; Turney, T.; Meredith, R.; Pan, Q.; Sernau, L.; Wang, X.; Hu, X.; Woods, R. J.; Carmichael, I.; Serianni, A. S. Submitted.
(42) Oborsky, P.; Tvaroska, I.; Králová, B.; Spiwok, V. *J. Phys. Chem. B* **2013**, *117*, 1003−1009.
(43) Babin, V.; Sagui, C. *J. Chem. Phys.* **2010**, *132*, 104108-1−104108-10.
(44) Ferro, D. R.; Provasoli, A.; Ragazzi, M.; Casu, B.; Torri, G.; Bossennec, V.; Perly, B.; Sinaÿ, P.; Petitou, M.; Choay, J. *Carbohydr. Res.* **1990**, *195*, 157−167.
(45) Sattelle, B. M.; Hansen, S. U.; Gardiner, J.; Almond, A. *J. Am. Chem. Soc.* **2010**, *132*, 13132−13134.
(46) Perlin, A. S.; Casu, B.; Sanderson, G. R.; Tse, J. *Carbohydr. Res.* **1972**, *21*, 123−132.
(47) Serianni, A. S.; Nunez, H. A.; Barker, R. *Carbohydr. Res.* **1979**, *72*, 71−78.
(48) Serianni, A. S.; Vuorinen, T.; Bondo, P. B. *J. Carbohydr. Chem.* **1990**, *9*, 513−541.
(49) Angyal, S. J.; Bethell, G. S.; Beveridge, R. J. *Carbohydr. Res.* **1979**, *73*, 9−18.
(50) King-Morris, M. J.; Bondo, P. B.; Mrowca, R. A.; Serianni, A. S. *Carbohydr. Res.* **1988**, *175*, 49−58.
(51) Austin, P. W.; Hardy, F. E.; Buchanan, J. C.; Baddiley, J. *J. Chem. Soc.* **1963**, 5350−5353.
(52) Hodge, J. E.; Hofreiter, B. T. *Methods Carbohydr. Chem.* **1962**, *1*, 380−394.
(53) Bock, K.; Pedersen, C. *Adv. Carbohydr. Chem. Biochem.* **1983**, *41*, 27−66.
(54) Tropper, F. D.; Andersson, F. O.; Grand-Maitre, C.; Roy, R. *Carbohydr. Res.* **1992**, *229*, 149−154.
(55) *MacNUTs Pro*; Acorn NMR, Inc.: Livermore, CA, 2001.
(56) Frisch, M. J. et al. *Gaussian 09*, Revision A.1; Gaussian, Inc., Wallingford, CT, 2009.
(57) Becke, A. D. *J. Chem. Phys.* **1993**, *98*, 5648−5652.
(58) Hehre, W. J.; Ditchfield, R.; Pople, J. A. *J. Chem. Phys.* **1972**, *56*, 2257−2261.
(59) Cancés, M. T.; Mennucci, B.; Tomasi, J. *J. Chem. Phys.* **1997**, *107*, 3032−3041.
(60) Cammi, R.; Mennucci, B.; Tomasi, J. *J. Phys. Chem. A* **2000**, *104*, 5631−5637.
(61) Sychrovsky, V.; Grafenstein, J.; Cremer, D. *J. Chem. Phys.* **2000**, *113*, 3530−3547.
(62) Helgaker, T.; Watson, M.; Handy, N. C. *J. Chem. Phys.* **2000**, *113*, 9402−9409.
(63) Barone, V.; Peralta, J. E.; Contreras, R. H.; Snyder, J. P. *J. Phys. Chem. A* **2002**, *106*, 5607−5612.

DOI: 10.1021/acs.joc.6b02399
J. Org. Chem. 2017, 82, 1356−1370